Lithos 140-141 (2012) 86–102

Contents lists available at SciVerse ScienceDirect

Lithos

journal homepage: www.elsevier.com/locate/lithos

# Late Carboniferous high $\varepsilon_{Nd}(t)$–$\varepsilon_{Hf}(t)$ granitoids, enclaves and dikes in western Junggar, NW China: Ridge-subduction-related magmatism and crustal growth

Gong-Jian Tang [a,b], Qiang Wang [a,*], Derek A. Wyman [c], Zheng-Xiang Li [d], Zhen-Hua Zhao [a], Yue-Heng Yang [e]

[a] State Key Laboratory of Isotope Geochemistry, Guangzhou Institute of Geochemistry, Chinese Academy of Sciences, Guangzhou 510640, China
[b] Graduate University of Chinese Academy of Sciences, Beijing 100049, China
[c] School of Geosciences, The University of Sydney, NSW 2006, Australia
[d] The Institute for Geoscience Research (TIGeR), Department of Applied Geology, Curtin University, GPO Box U1987, Perth, WA 6845, Australia
[e] Institute of Geology and Geophysics, Chinese Academy of Sciences, Beijing 100029, China

ARTICLE INFO

*Article history:*
Received 3 September 2011
Accepted 27 January 2012
Available online 3 February 2012

*Keywords:*
Granitoid
Enclave
Dike
Crustal growth
Ridge subduction
Central Asian Orogenic Belt

ABSTRACT

We report results of petrologic, geochronological and geochemical investigation of the Late Carboniferous diorites, granodiorites, amphibole (Am)-bearing granites, and associated dioritic and monzonitic enclaves and mafic and granitic dikes in the Keramay area, of the western Junggar region of Central Asian Orogenic Belt (CAOB). Zircon U–Pb dating suggests that they were generated in the Late Carboniferous (316–304 Ma). The diorite and granodiorite compositions extend over a wide range of $SiO_2$ (53–70 wt.%), Sr (240–602 ppm), and $Mg^{\#}$ (41–58) values, and are characterized by moderately fractionated rare earth element (REE) patterns, Nb–Ta depletion and relatively low Y and Yb contents. The mafic dikes consist of dolerites, diorite porphyries and minor granodiorite porphyries, and have variable $SiO_2$ (51–59 wt.%) and high $Mg^{\#}$, Cr and Ni values. With the exception of two samples with relatively high heavy REE (HREE) contents, the mafic dikes exhibit trace element characteristics similar to diorites and granodiorites. The Am-bearing granites and a granite porphyry dike sample have high levels of $SiO_2$ (73–77 wt.%), HREEs (e.g., Yb = 3.46–15.7 ppm) and low $Mg^{\#}$, Cr and Ni contents, along with clearly negative Eu, Ba and Sr anomalies, similar to typical A-type granites. All granitoids, enclaves and dikes in this region have high positive $\varepsilon_{Nd}(t)$ (+7.13 to +9.74) and zircon $\varepsilon_{Hf}(t)$ (+10 to +16) values and moderate initial $^{87}Sr/^{87}Sr$ ratios (0.7004–0.7049). Mineral composition data suggest that the parental magmas for mafic dikes are similar to Cenozoic sanukitoids in the Setouchi arc area (Japan) and were possibly generated under water-rich and high oxygen fugacity (NNO + 1.5 to NNO + 2.7) conditions. They most likely originated from partial melting of a mantle source variably modified by subducted oceanic crust-derived melts and minor fluids and subsequently underwent fractional crystallization. The diorites and granodiorites were possibly generated by magma mixing between enriched lithospheric mantle and juvenile lower crust-derived magmas coupled with minor crystal fractionation. The Am-bearing granites and granite porphyry dike were produced by partial melting of juvenile crustal materials at shallow crustal levels. Taking into account widespread contemporaneous magmatism including "MORB-type" basalts and slab-derived adakites in western Junggar, we suggest that the Keramay intrusive rocks were generated in a special arc setting related to ridge subduction and resultant slab window, which played an important role in the crustal growth of the CAOB.

© 2012 Elsevier B.V. All rights reserved.

## 1. Introduction

Crustal growth and the associated process of extracting material from the mantle are major issues in Earth's history (Reymer and Schubert, 1986; Rudnick, 1995; Taylor and McLennan, 1995). However, the models for crustal growth have been the subject of a long-standing debate. Possible models include lateral accretion of arc complexes in subduction zones (Davidson and Arculus, 2006; Taylor and McLennan, 1985), vertical addition of mafic magma underplating at the crust–mantle interface (Frost et al., 2001), involvement of hotspots or mantle plumes (e.g., oceanic plateaus and continental flood basalts) (Albarède, 1998; Condie, 2000; Hawkesworth and Kemp, 2006; Kemp et al., 2006; Kerr et al., 2009; Mann and Taira, 2004), and a combination of subduction and plumes (Lapierre et al., 2003; Wyman, 1999; Wyman and Kerrich, 2009).

Koto (1916) first applied the term "sanukitoid" to all textural variations of volcanic rocks with the composition of Weinschenk's sanukite suite (bronzite-bearing glassy aphyric andesite) (Weinschenk, 1891). Tatsumi and Ishizaka (1981) used the term "sanukitoid" for a variety of relatively aphyric basalts and andesites with less than

* Corresponding author. Tel.: +86 20 85290277; fax: +86 20 85290130.
*E-mail address:* wqiang@gig.ac.cn (Q. Wang).

0024-4937/$ – see front matter © 2012 Elsevier B.V. All rights reserved.
doi:10.1016/j.lithos.2012.01.025

20 vol.% phenocrysts. Shirey and Hanson (1984) proposed the term "Archean sanukitoid" for a variety of Archean high-Mg granitoids (diorites, monzodiorites, monzonites and trachyandesites) because of their chemical similarity to Miocene sanukitoids in the Setouchi Volcanic Belt, Southwestern Japan (Tatsumi and Ishizaka, 1981). Recently, sanukitoids have been widely used to include all volcanic and intrusive rocks with geochemical characteristics similar to these Japanese sanukitoids (Martin et al., 2005; Stern et al., 1989; Tatsumi, 2008). They are commonly related to subduction and slab breakoff tectonic settings, although plume-related origins have also been suggested, and are generally considered to require the involvement of both crustal and mantle components (Halla et al., 2009; Heilimo et al., 2010; Lobach-Zhuchenko et al., 2008; Wang et al., 2011; Whalen et al., 2004; Smithies et al., 2007). They are widely observed in Archean terranes but are also associated with present-day warm-slab and hot-mantle-wedge environments, and resemble the continental crust in composition (Kelemen, 1995; Tatsumi, 2006, 2008). However, granitoids with non-sanukitoid compositions are the most common rocks in the continental crust. Consequently, continental growth may largely hinge on processes involved in sanukitoid and granitoid generation. Mafic enclaves and dikes that occur in granitoids, particularly calc-alkaline granitoids, provide significant information on their sources and formation mechanisms and clarify the interaction between crust- and mantle-derived magmas.

The Central Asian Orogenic Belt (CAOB), also known as "the Altaid Tectonic Collage", is an immense accretionary orogen (Fig. 1a) and is an important site of Phanerozoic crustal growth (Jahn, 2004; Sengör et al., 1993; Windley et al., 2007). Granitoids with highly depleted isotopic signatures are widespread in the CAOB (Chen and Arakawa, 2005; Chen and Jahn, 2004; Jahn, 2004; Jahn et al., 2000, 2004; Wu et al., 2000; 2002). It is widely accepted that these granitoids signify crustal growth, but the petrogenesis and geodynamic setting of these rocks and the associated modes for crustal growth in the CAOB are the subjects of an ongoing debate. One view holds that nearly half of the CAOB was derived from the mantle by successive accretion of arc complexes and subduction accretion during the

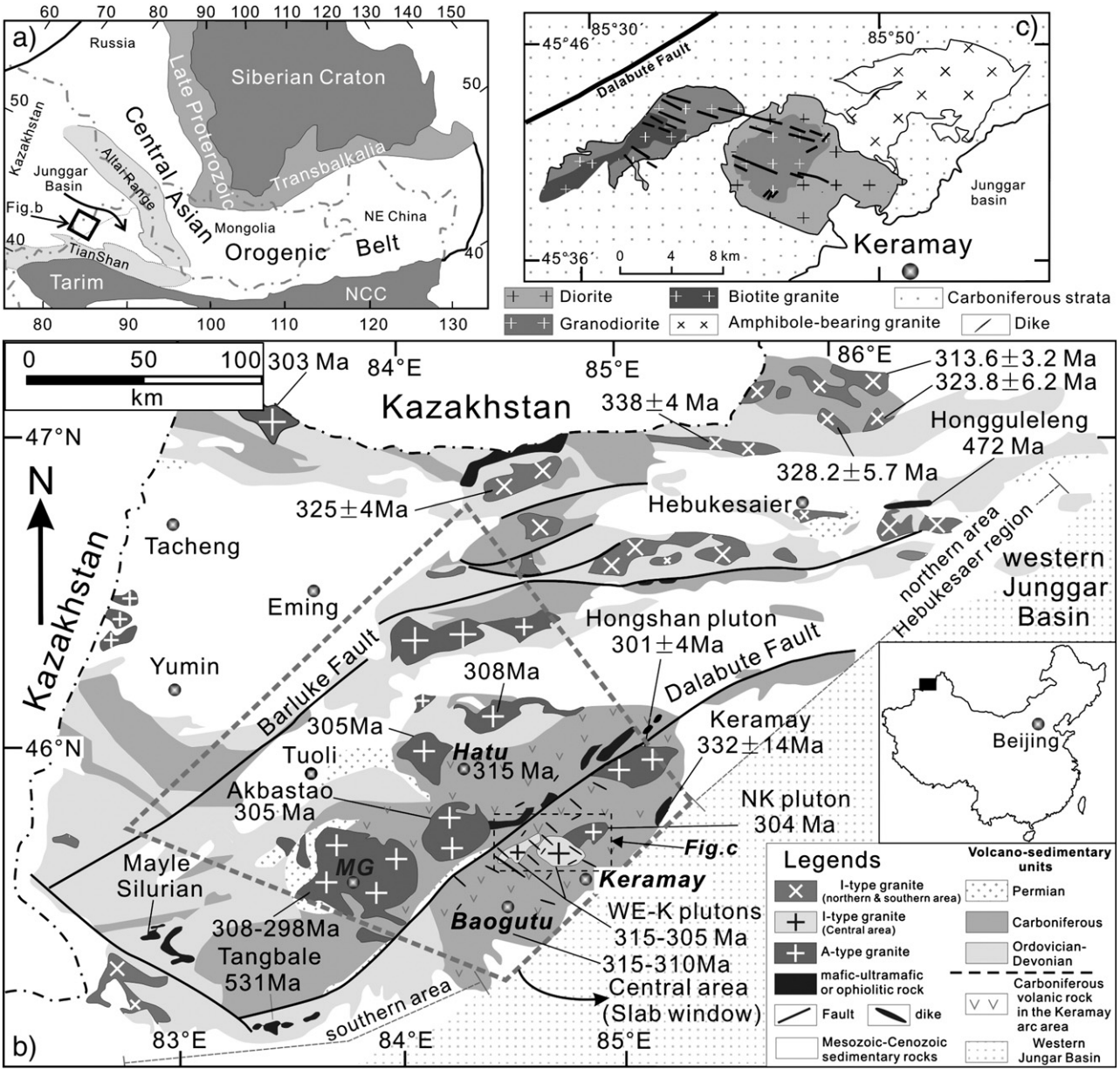


**Fig. 1.** (a) Simplified tectonic divisions of the CAOB (after Jahn et al., 2000). (b) Geological map of the western Junggar region (Tang et al., 2010). (c) Simplified geological map of the Keramay plutons and dikes.

Phanerozoic (Sengör et al., 1993). Other models suggest that Phanerozoic CAOB granitoids were generated by basalt underplating in a post-collisional setting (Jahn et al., 2000; Wu et al., 2000). Recently, Windley et al. (2007) proposed many diagnostic features that are explicable by ridge subduction in the CAOB, and some other researchers have also proposed important contributions from Paleozoic ridge subduction in the region (Geng et al., 2009; Jian et al., 2008; Liu et al., 2007; Tang et al., 2010; Yin et al., 2010; Zhang et al., 2011a, 2011b).

The western Junggar region in the southwestern part of the CAOB is considered to be an important area for Phanerozoic crustal growth owing to the presence of large scale granitoids with high and positive $\varepsilon_{Nd}(t)$ values (>+6.0) (Chen and Arakawa, 2005; Geng et al., 2009; Tang et al., 2010). In this study, we present combined *in situ* zircon U–Pb age and Hf isotope data, mineral compositions, whole rock geochemical and Sr–Nd isotopic data for mafic and granite porphyry dikes, diorites, granodiorites and their mafic enclaves, and amphibole (Am)-bearing granites and their monzonitic enclaves in the western Junggar region from the southwestern CAOB (Fig. 1). These data are used to document the emplacement ages and petrogenesis of these rocks, constrain the associated geodynamic processes, and evaluate the implications for crustal growth.

## 2. Geological setting and pluton petrological characteristics

The CAOB extends from the Urals in the west, through Kazakhstan, northern China, Mongolia, and southern Siberia to the Okhotsk Sea along the eastern Russian coast (Fig. 1a) (Jahn, 2004; Sengör et al., 1993; Xiao et al., 2003). It is located between the Siberian Craton to the north and the North China and Tarim cratons to the south (Fig. 1a). The main period of crustal evolution in the CAOB began at ca. 1.0 Ga (Khain et al., 2002; Kovalenko et al., 2004) and continued to the end of the Permian (Xiao et al., 2003) with voluminous juvenile granitoids emplaced throughout the CAOB. The western Junggar, in the southwestern CAOB, is surrounded by the Tianshan Orogen to the south, the Altai Orogen to the north, the Kazakhstan Plate to the west, and the Junggar Basin to the east (Fig. 1a). Many ophiolitic mafic–ultramafic rocks with ages ranging from the Cambrian to Early Carboniferous occur in the western Junggar region (Xiao et al., 2008), but no metamorphic basement has been documented. Volcanic–sedimentary strata in the region are dominantly Devonian to Carboniferous in age (Fig. 1b). Carboniferous to Early Permian magmatic rocks, especially granitoids, occur widely in the western Junggar region and are referred to here as the Keramay arc magmatic rocks (Tang et al., 2010). In the central area of the western Junggar region (Keramay–Hatu area), both large batholiths and relatively small stocks intrude the Carboniferous strata (Fig. 1b). Volcanic rocks and mafic dikes are also abundant in the central part of the western Junggar region (Fig. 1b). Scattered occurrences of volcanic rocks across the western Junggar region were erupted at ca. 350–315 Ma and consist of andesitic basalts, andesites, felsic tuffs and minor quartz or olivine tholeiites (Geng et al., 2011; Tang et al., 2012; Wang and Zhu, 2007). Numerous mafic dikes and smaller numbers of felsic dikes mainly strike NW (280°–300°) and cut both granitoid intrusions and the Carboniferous strata (Yin et al., 2010).

The compositionally diverse Keramay plutons are located to the east of the Dalabute fault and occupy an area that is ~40 km long and has a maximum width of 16 km. They include the North Keramay (NK), East Keramay (EK) and West Keramay (WK) plutons (Fig. 1c). The petrological characteristics of these plutons are shown in Fig. 2a–h and Appendix 1.

The EK and WK plutons include similar rock types: gabbroic diorites (0–1 vol.%), diorites (52 vol.%), granodiorites (36 vol.%), biotite granites (11 vol.%), and their mafic enclaves (0–1 vol.%) (Fig. 2a). The intrusive rocks share some common petrographic features, and consist essentially of plagioclase, K-feldspar, quartz, biotite, and amphibole, and accessory phases (magnetite, apatite, titanite and zircon) (Fig. 2a and g). Most of mafic enclaves are circular, elliptical or drop-like and have either sharp or diffuse boundaries with their host granitoids. Mineralogically, they are classified as diorites and quartz diorites. They contain more ferromagnesian minerals (amphibole), plagioclase, and less quartz and K-feldspar than their host granitoids. Some of the amphiboles are acicular and the enclaves also contain acicular apatite (Fig. 2h). No cumulate textures are found in the mafic enclaves. Some mafic dikes intrude into the EK and WK plutons and Carboniferous strata. They are variable in size but most are 0.5–3.0 m wide and less than 1 km long (Fig. 2b). The dikes include dolerites, diorite porphyrites and minor granodiorite porphyrites, with diabasic and porphyritic texture, and mainly consist of plagioclase, amphibole, pyroxene, biotite and magnetite (Fig. 2f).

The NK pluton mainly comprises Am-bearing alkali-feldspar granites; sporadic monzonitic enclaves and dikes occur in the pluton. Some granite porphyry dikes intrude into the Carboniferous strata near the NK pluton. The Am-bearing granites of the NK pluton consist of alkali feldspar, quartz, plagioclase, biotite, hornblende, and accessory minerals including zircon, apatite and magnetite (Fig. 2c, d, e). Enclaves in the NK pluton show sharp contact relationships with the host (Fig. 2c). The enclaves consist of hornblende, biotite, plagioclase, K-feldspar, quartz, and accessory minerals, similar to those in their host Am-bearing granites. The granite porphyry has a fine-grained porphyritic texture, and contains K-feldspar, quartz, plagioclase, and accessory minerals of zircon, apatite and magnetite.

## 3. Analytical results

Analytical methods used for the determination of whole-rock major and trace element abundances and Sr–Nd isotope compositions, mineral chemical compositions and zircon U–Pb ages and Lu–Hf isotope compositions are presented in Appendix 2, and related analytical data are listed in Appendices 3–8.

### 3.1. Mineral composition

#### 3.1.1. Clinopyroxene

Clinopyroxene grains from mafic dikes have $Mg^{\#}$ values ($Mg/(Mg+Fe^{2+})$, of 0.69–0.92 and variable $Al_2O_3$ and $TiO_2$ contents (1.8–6.2 wt.% and 0.3–1.2 wt.%, respectively). Clinopyroxene compositions are $Wo_{24-47}En_{40-49}Fs_{10-24}$, corresponding to diopside and augite (Fig. 3; Appendix 3).

#### 3.1.2. Amphibole

Using the classification of Leake et al. (1997), Mg-hornblende mainly occurs in mafic dikes, diorites, granodiorites and dioritic enclaves, Mg-pargasite and edenite in diorites and granodiorites, and actinolite and pargasite in mafic dikes, respectively (Fig. 3; Appendix 3). The amphibole $Mg^{\#}$ ($Mg/(Mg+Fe2^{+})$) ratios from the mafic dikes range from 0.76 to 0.91, which is slightly higher than those from diorites and granodiorites (0.53–0.73) or their dioritic enclaves (0.66–0.76). Amphiboles in the Am-bearing granites and their monzonitic enclaves plot in the field of Fe-edenite (Fig. 3; Appendix 3). They show distinctive low $Mg^{\#}$ (ratios, varying from 0.29 to 0.35 and 0.34 to 0.40, respectively.

#### 3.1.3. Biotite

The brown micas from the diorites and granodiorites are Mg-biotites (Foster, 1960; Rieder et al., 1998), with high $Mg/(Mg+Fe)$ ratios of ~0.51 together with low F contents (0.04–0.18 wt.%) (Fig. 3; Appendix 3). Micas within Am-bearing granites and their monzonitic enclaves are Fe-biotites, with low $Mg^{\#}$ ($Mg/(Mg+Fe)$)

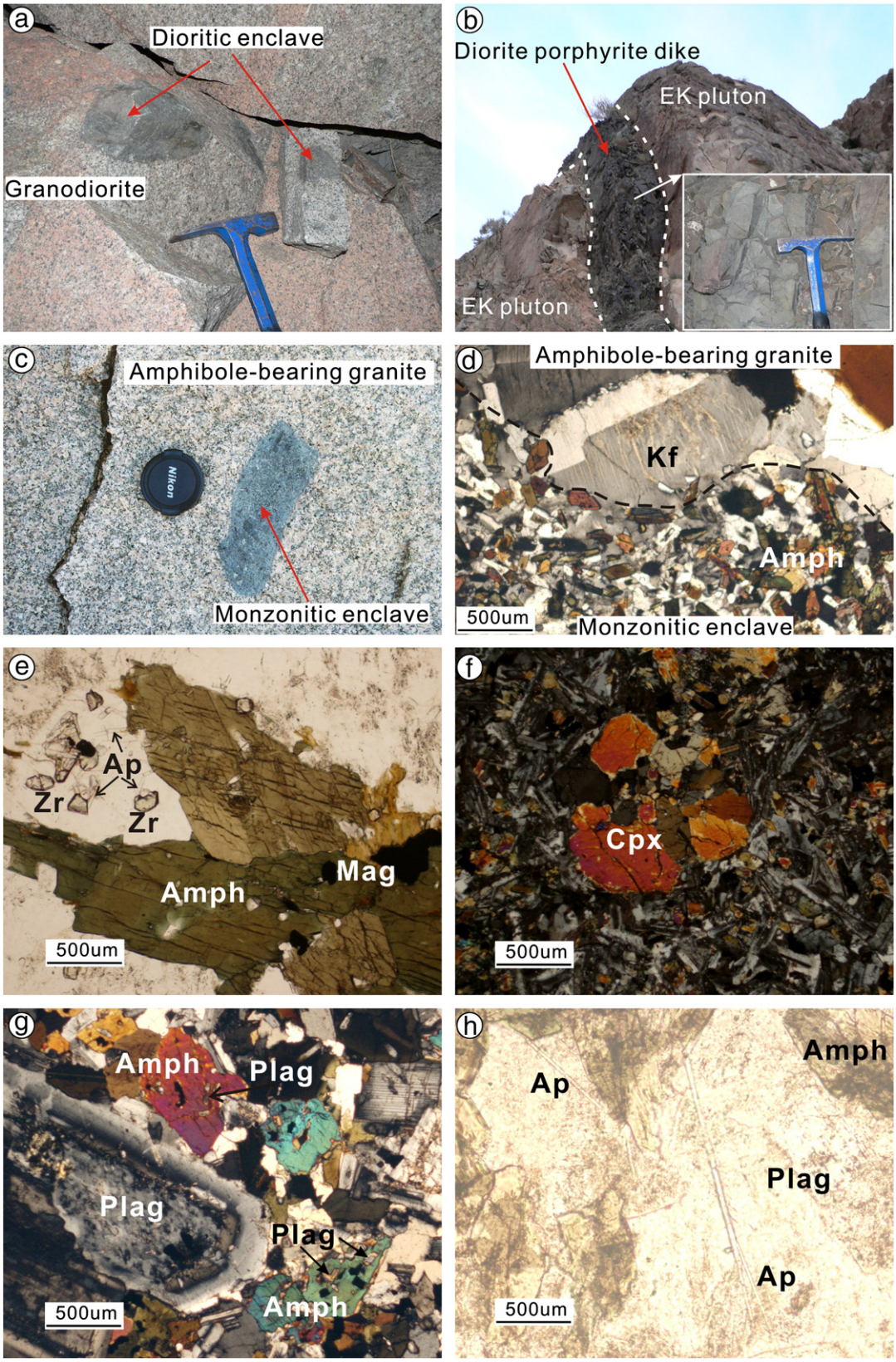


**Fig. 2.** Field photographs showing (a) dioritic enclaves in the West-Keramay pluton, (b) the diorite porphyrite dike intruded into the East-Keramay pluton, (c) the sampled monzonitic enclave occurring within North-Keramay pluton. Microphotographs showing (d) the boundary between the Am-bearing granite and its monzonitic enclave; (e) amphibole, zircon and apatite in the Am-bearing granite; (f) clinopyroxene crystals in a mafic dike; (g) plagioclase in diorite from EK pluton showing complex oscillatory zoning. Plagioclase and magnetite mineral inclusions in large hornblende crystals from the diorite; (h) acicular apatite within the mafic enclave in the East-Keramay pluton. Amph-Amphibole; Ap = Apatite; Cpx = Clinopyroxene; Kf = K-feldspar; Mag = Magnetite; Plag = Plagioclase; Zr = Zircon.

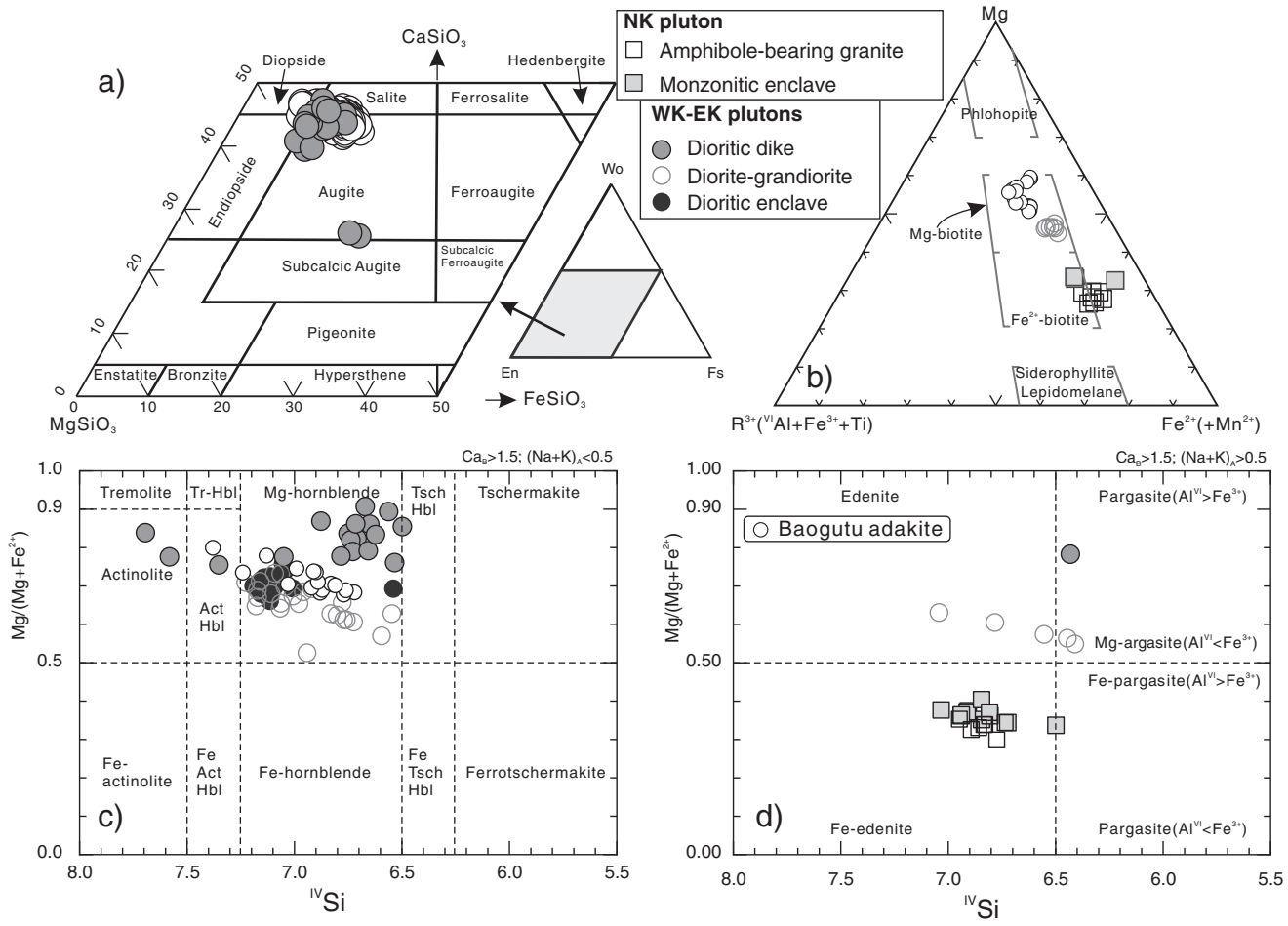


**Fig. 3.** (a) $CaSiO_3$–$MgSiO_3$–$FeSiO_3$ diagram showing the compositions of pyroxene (Morimoto et al., 1988). (b) $Mg$–$R^{3+}$–$Fe^{2+}$ ($+Mn^{2+}$) classification diagram for micas (Foster, 1960). (c and d) Classification of calcic amphibole in terms of Si versus $Mg/Mg+Fe^{2+}$, according to the recommended IMA criteria (Leake et al., 1997).

ratios ranging from 0.29 to 0.32 and 0.35 to 0.36 together with high F contents (0.92–1.42 wt.%; 1.08–1.55 wt.%), respectively. The $Al_2O_3$ and $TiO_2$ contents of these biotites show a narrow range (Appendix 3). The compositions of igneous biotites reflect the nature of their host parental magmas and can be used to discriminate anorogenic alkaline, peraluminous and calc-alkaline suites in granitoids (Abdel Rahman, 1994). Biotites from the calc-alkaline diorites and granodiorites from EK–WK plutons are moderately enriched in MgO and $Al_2O_3$, but depleted in FeO than those from the Am-bearing granites and their monzonic enclave from NK pluton, and plot in the field of metaluminous calc-alkaline granites. In contrast, biotites of NK pluton plot in the field of anorogenic alkaline granites (Fig. 4).

### 3.1.4. Feldspar

Plagioclases and K-feldspars occur in all of the granitoids from the Keramay plutons. The plagioclases are represented by a wide range of

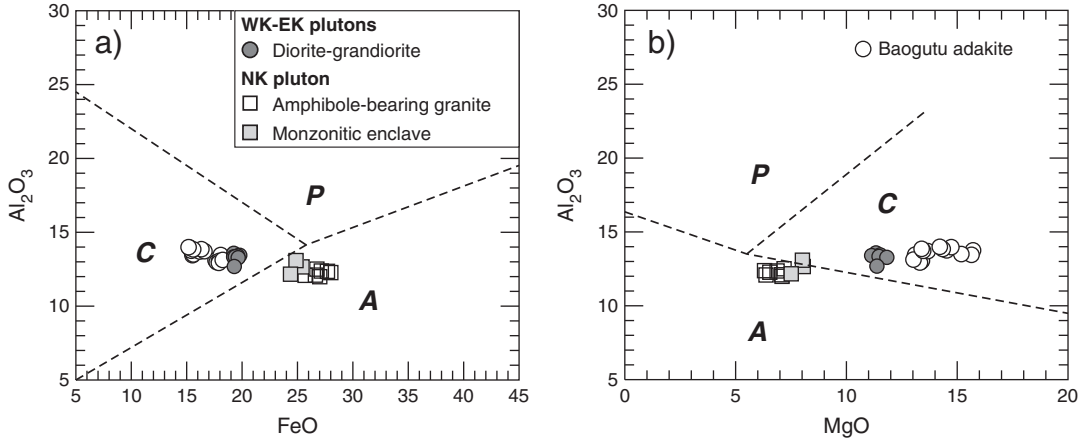


**Fig. 4.** FeO–$Al_2O_3$–MgO diagrams for the biotite (after Abdel Rahman, 1994). A: biotite in anorogenic alkalines suites; P: biotite in peraluminous granites (S-type granites); C: biotite in metaluminous calc-alkaline granites suite (I-type granites).

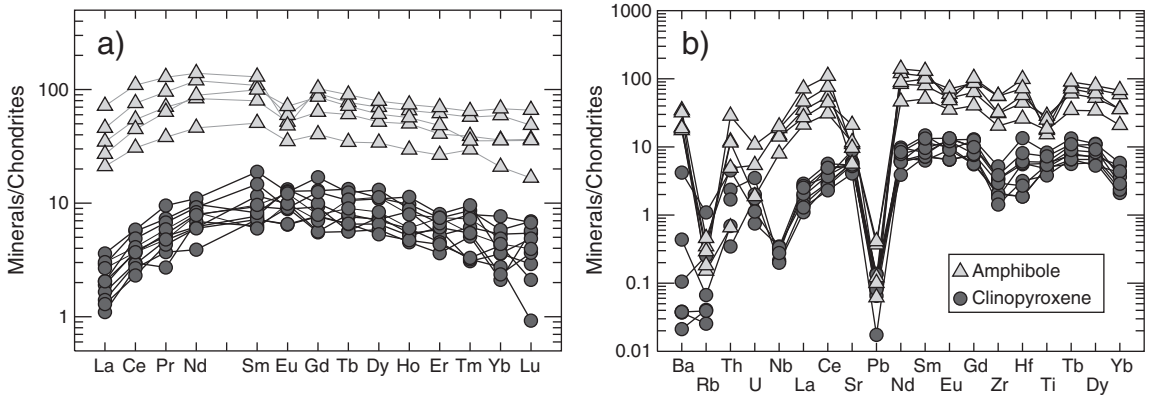


**Fig. 5.** Chondrite-normalized REE and incompatible element patterns for amphibole and clinopyroxene grains from the mafic dikes. The chondrite values are from Sun and McDonough (1989).

compositions from labradorite (An60) to oligoclase (An21) from the diorites. K-feldspar compositions within the Am-bearing granites are characterized by a variation in orthoclase and albite contents ranging from $Or_{78}$ to $Or_{91}$ and $Ab_9$ to $Ab_{21}$, respectively, corresponding to anorthoclase (Appendix 3).

*3.1.5. Trace element compositions of clinopyroxene and amphibole from mafic dikes*

Clinopyroxenes from the mafic dikes are characterized by light REE (LREE) depletion ($La_N/Sm_N = 0.12–0.35$, for $Sm_N = 6–19$) and fractioned HREE ($Sm_N/Yb_N = 1.4–4.2$), with slightly negative to positive Eu anomalies and Nb and Zr depletions (Fig. 5). The clinopyroxenes can be divided into two groups based on their Ba concentrations. The high-Ba (~10 ppm) group also has high Rb, Th and U concentrations with low Cr contents ranging from 574 to 741 ppm; Th and U are variably enriched over Nb but similar to Ba. However, the low-Ba (≤1 ppm) group has low Rb and high Th and U contents with high Cr contents varying between 1066 and 3568 ppm.

The chondrite-normalized REE patterns of amphiboles are characterized by slightly fractioned LREE and HREE ($La_N/Sm_N = 0.27–0.55$; $Sm_N/Yb_N = 1.9–2.8$), with negative to negligible Eu anomalies. The incompatible element patterns reveal significant Rb, Pb, Zr and Ti,

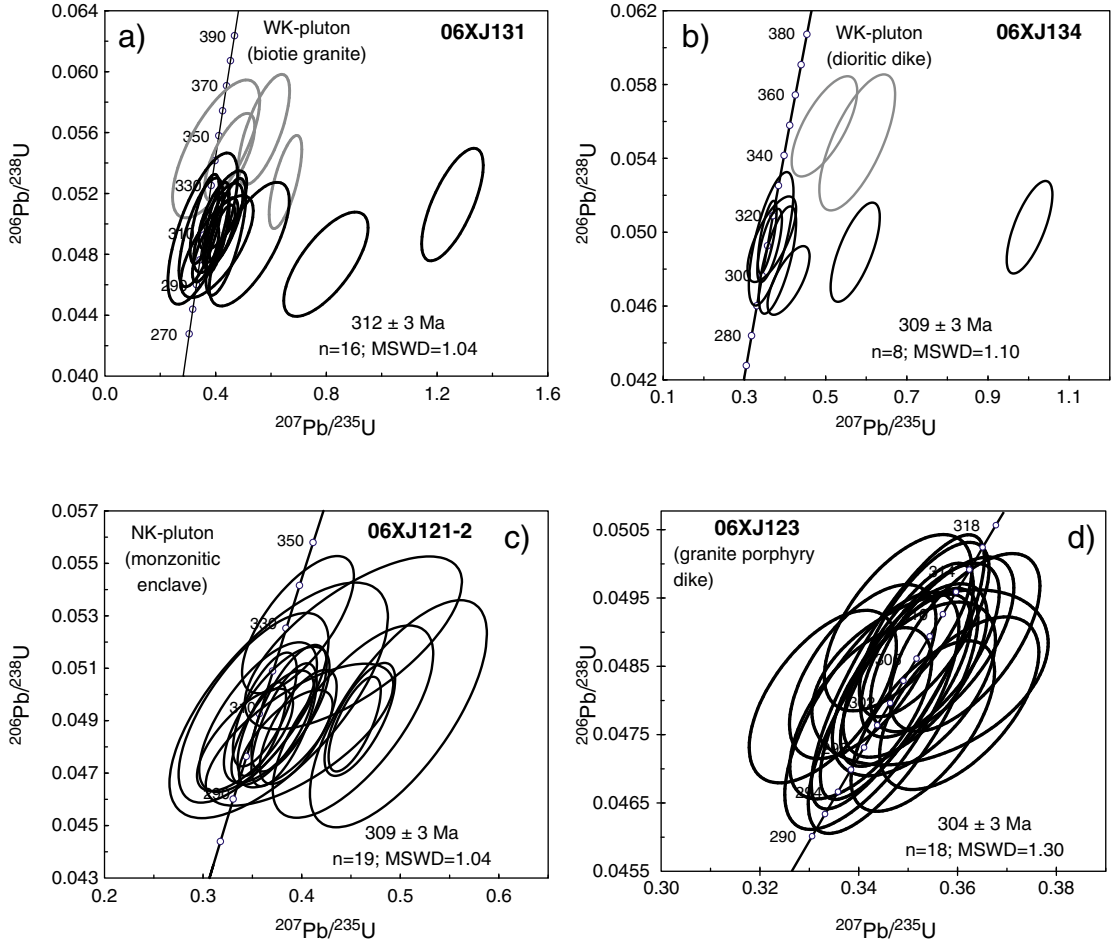


**Fig. 6.** Concordia diagrams of LA-ICPMS (a–c) and SHRIMP (d) zircon U–Pb analyses for the granitoids, dikes and mafic enclaves in the Keramay area (western Junggar).

and slight Nb and Ta depletions. Their Th and U concentrations are highly scattered. The amphiboles have low Cr contents (1.8–64 ppm).

### 3.2. U–Pb zircon geochronology

#### 3.2.1. WK and EK plutons

Zircon grains from the WK pluton (06XJ131, biotite granite) and a dioritic dike (06XJ134) occurring in this pluton show internal oscillatory zonation. They are 60–120 μm long and are mostly subhedral–euhedral prismatic crystals. They have highly variable U (303–1082 ppm, 303–1968 ppm) and Th (140–670 ppm, 140–4255 ppm) contents, with Th/U ratios ranging from 0.31 to 2.12, indicative of a magmatic origin (Belousova et al., 2002). Fifteen and eight analyses form a coherent group and define a weighted mean $^{206}Pb/^{238}U$ age of 311 ± 3 Ma and 309 ± 3 Ma for samples 06XJ131 and 06XJ134, respectively (Fig. 6). Moreover, four other analyses give $^{206}Pb/^{238}U$ ages of 331 Ma and 352 Ma for the biotite granite sample and two other analyses give $^{206}Pb/^{238}U$ ages of 344 Ma and 350 Ma for the dike sample, respectively. These old zircons were likely inherited from their source or entrained from the wall rocks during emplacement. The granodiorites and diorites from the EK pluton formed at 316 ± 3 Ma and 314 ± 3 Ma, respectively (Tang et al., 2012).

#### 3.2.2. NK pluton

Zircon grains from one monzonitic enclave sample (06XJ121-2) in the NK pluton are stubby and prismatic, generally with lengths of 70–150 μm. Most grains are transparent and exhibit concentric compositional zoning. These zircons are characterized by high U (303–1803 ppm) and Th (140–670 ppm) contents with relatively high Th/U ratios (0.22–0.61). Nineteen zircon grains from the monzonitic enclave form a single population and yield a weighted mean $^{206}Pb/^{238}U$ age of 309 ± 3 Ma (Fig. 6), which is identical to the formation age (304 ± 3 Ma) of the Am-bearing granites host rocks (Tang et al., 2012).

#### 3.2.3. Granitic porphyry dike

Cathodoluminescence (CL) images show that zircon grains from the felsic dike (06XJ123) are prismatic and euhedral crystals with rhythmic oscillatory zoning and lengths of generally 50 to 100 μm long. The zircon grains have U contents ranging from 670 to 1342 ppm and Th contents ranging from 311 to 598 ppm, with relatively low and consistent Th/U ratios (0.45–0.56). Eighteen analyses yield $^{206}Pb/^{238}U$ ages between 301 ± 3 Ma and 310 ± 3, with a weighted mean $^{206}Pb/^{238}U$ age of 305 ± 3 Ma (Fig. 6). This is interpreted as the best estimate of the time of crystallization of the felsic dike.

### 3.3. Geochemistry and isotopic compositions

#### 3.3.1. Major and trace elements

All of the samples are subalkaline and plot in the fields of gabbroic diorites, diorites, granodiotites or granites (Fig. 7a). The diorite and granodiorite samples have widely varying $SiO_2$ contents (53.36–70.03 wt.%), and the biotite granite sample has an $SiO_2$ content of 75.12 wt.%. They have moderate total alkali ($Na_2O + K_2O$ = 4.34–7.85 wt.%) contents, with $Na_2O/K_2O$ ratios near or more than 1 (Fig. 7b). They have variable MgO (0.34–5.81 wt.%), total FeO (0.75–7.65 wt.%), Cr (0.92–95.3 ppm) and Ni (3.99–69.2 ppm) contents (Fig. 8; Appendix 6). One dioritic enclave sample in the granodiorites has low $SiO_2$ content (51.48 wt.%), with relatively higher total alkali ($Na_2O + K_2O$ = 5.83 wt.%) content and high $Na_2O/K_2O$ ratio of 2.6 (Fig. 7). On the selected oxides and trace elements vs. MgO diagrams (Fig. 8), $SiO_2$, total alkalis, Ba and Th abundances for diorites and granodiorites and their enclave increase, whereas, their compatible oxides and elements ($TiO_2$, total FeO, V, Cr and Ni), and CaO abundances, along with CaO/$Al_2O_3$ and $Na_2O/K_2O$ ratios, decrease with decreasing MgO contents, defining a linear trend. The dioritic enclave has higher MgO, $TiO_2$, $Al_2O_3$, total FeO, CaO, $K_2O + Na_2O$, Cr, Ni and Sr contents than those of the host intrusive rocks. The diorite and granodiorite samples have moderate Sr concentrations (240–602 ppm), Sr/Y ratios are also moderate (16–40). By comparison, the diorite enclave has higher Sr content (673 ppm) and higher Sr/Y ratio of 41.4 (Appendix 6). Except for the high-$SiO_2$ biotite granite (06XJ131) $\left(Eu/Eu^* \left(= Eu_N / \sqrt[2]{Sm_N \times Gd_N}\right) = 0.65\right)$, all rocks show only insignificant negative Eu anomalies ($Eu/Eu^* = 0.85 \pm 0.05$), contrasting with the significant positive Eu anomaly ($Eu/Eu^* = 1.25$) of the dioritic enclave (Fig. 9). On primitive mantle normalized multi-element diagrams, they are enriched in large ion lithophile elements (LILEs) (e.g., Rb, Ba, Th, and U) and depleted in Nb, Ta, P and Ti. In addition, they exhibit weakly negative to positive Sr anomalies (Fig. 9). The dioritic enclave shows trace element characteristics similar to its host rocks, except for a weakly positive Ti anomaly.

The mafic dikes are basic to intermediate with $SiO_2$ ranging from 51.32 to 66.62 wt.%. They have variable and high MgO (1.19–7.41 wt.%) with relatively high $Al_2O_3$ (14.67–17.92 wt.%), $TiO_2$ (0.50–1.96 wt.%), Cr (3.99–446 ppm) and Ni (5.82–162 ppm) abundances, high $Na_2O/K_2O$ ratios of 1.4–5.7, but with low total alkalis ($Na_2O + K_2O$ = 3.1–3.6 wt.%). They have high Sr (589 ± 89 ppm) and Ba (416 ± 131 ppm) concentrations, with high Sr/Y ratios (43 ± 13) (Appendix 6). Except for two samples with relatively high heavy REE (HREE) contents, the mafic dikes exhibit trace element characteristics similar to diorites and

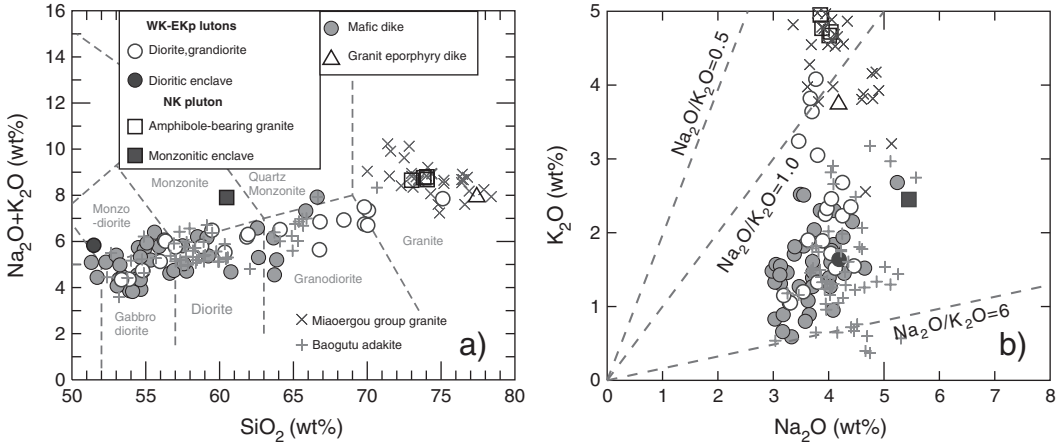


**Fig. 7.** Plots of (a) total alkalis vs. $SiO_2$, (b) $K_2O$ vs. $Na_2O$ for Late Carboniferous magmatic rocks from the granitoids, dikes and mafic enclaves in the Keramay area (western Junggar). Data sources are from Appendix 6, and Chen and Arakawa (2005), Li et al.(2004), and Yin et al.(2010).

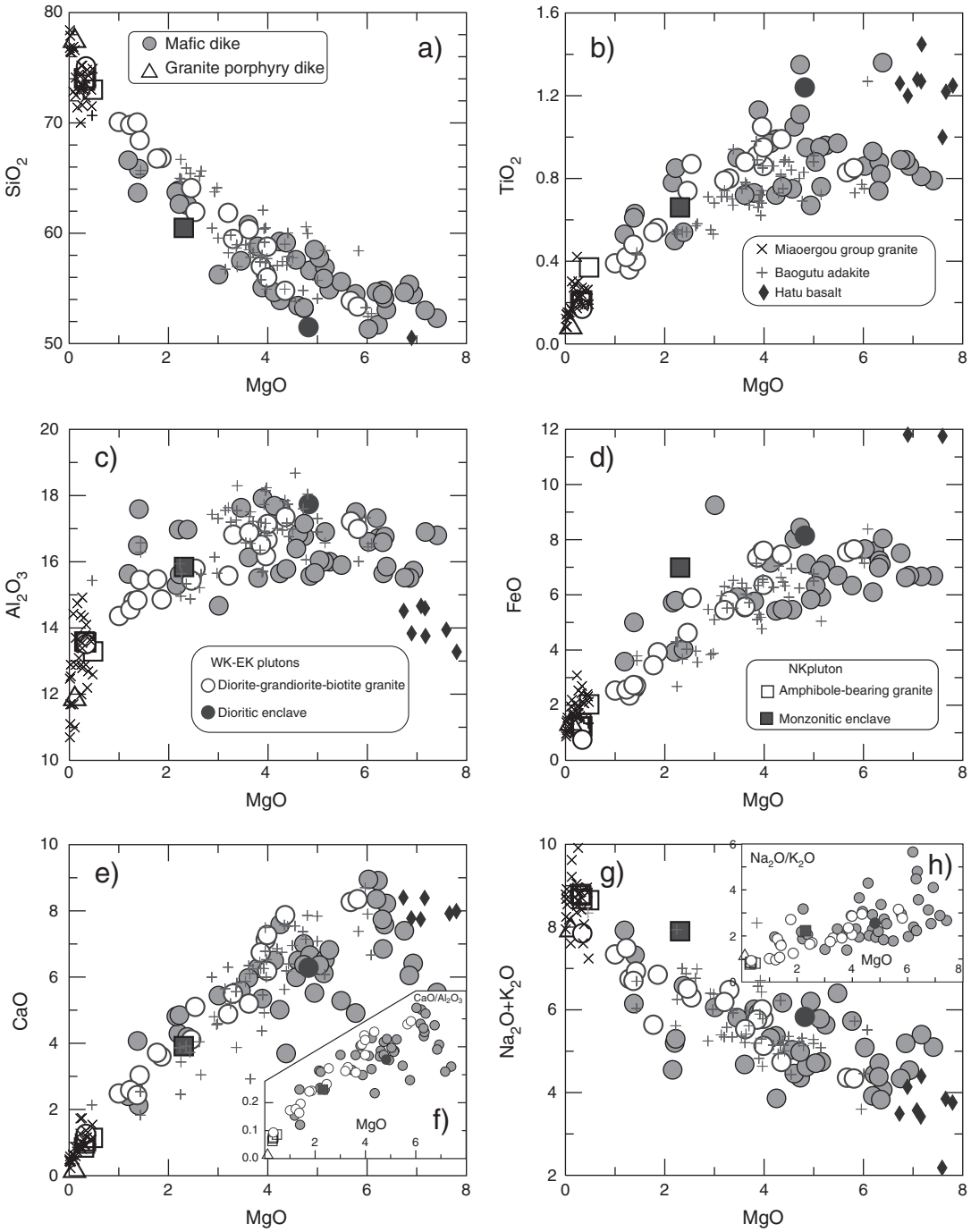


**Fig. 8.** Various oxides (wt.%) and trace elements (ppm) plots for the granitoids, dikes and mafic enclaves of the Keramay area (western Junggar).

granodiorites. Apart from the highest-$SiO_2$ sample (06XJ169) with $Eu/Eu^* = 0.58$, the mafic dikes have negligible Eu anomalies ($Eu/Eu^* = 0.99 \pm 0.12$) (Appendix 6; Fig. 9).

The Am-bearing granites of the NK pluton and the granite porphyry dike are high in silica and alkalis, with $SiO_2$ and total $K_2O + Na_2O$ varying from 73.01 to 77.42 wt.% and 7.93 to 8.80 wt.%, respectively. The Am-bearing granites have low $Na_2O/K_2O$ ratios ($0.83 \pm 0.04$), whereas, the granite porphyry dike has a $Na_2O/K_2O$ ratio slightly great than 1 (Fig. 7). The monzonitic enclave in the NK pluton has intermediate $SiO_2$ content (60.48 wt.%), with high total alkalis (7.91 wt.%) and $Na_2O/K_2O$ ratio (2.2). The Am-bearing granites and granite porphyry dike have low MgO, $Al_2O_3$, total FeO, Cr and Ni concentrations (Fig. 8). The Am-bearing granites are enriched in LREEs relative to heavy REEs with $(La/Yb)_N$ ratios of 4.6–7.3, whereas, the granite porphyry dike and monzonitic enclave have unfractionated REE with $(La/Yb)_N$ ratios of 1.0 and 1.1. All of these rock types exhibit strongly negative Eu anomalies ($Eu^* < 0.3$). Am-bearing granites and the related monzonitic enclave show similar characteristics on primitive mantle normalized multi-element diagrams, with negative Ba, U, Nb, Sr, P, Eu and Ti anomalies. The granitic porphyry dike is enriched in Rb, Th, U, Nb, Ta, Zr and Hf and depleted in Ba, Sr, P, Eu and Ti (Fig. 9).

### 3.3.2. Whole rock Sr–Nd isotopic data

Sr–Nd isotope compositions for granitoids, dikes and enclaves in the Keramay area are listed in Appendix 7 and plotted on Fig. 10.

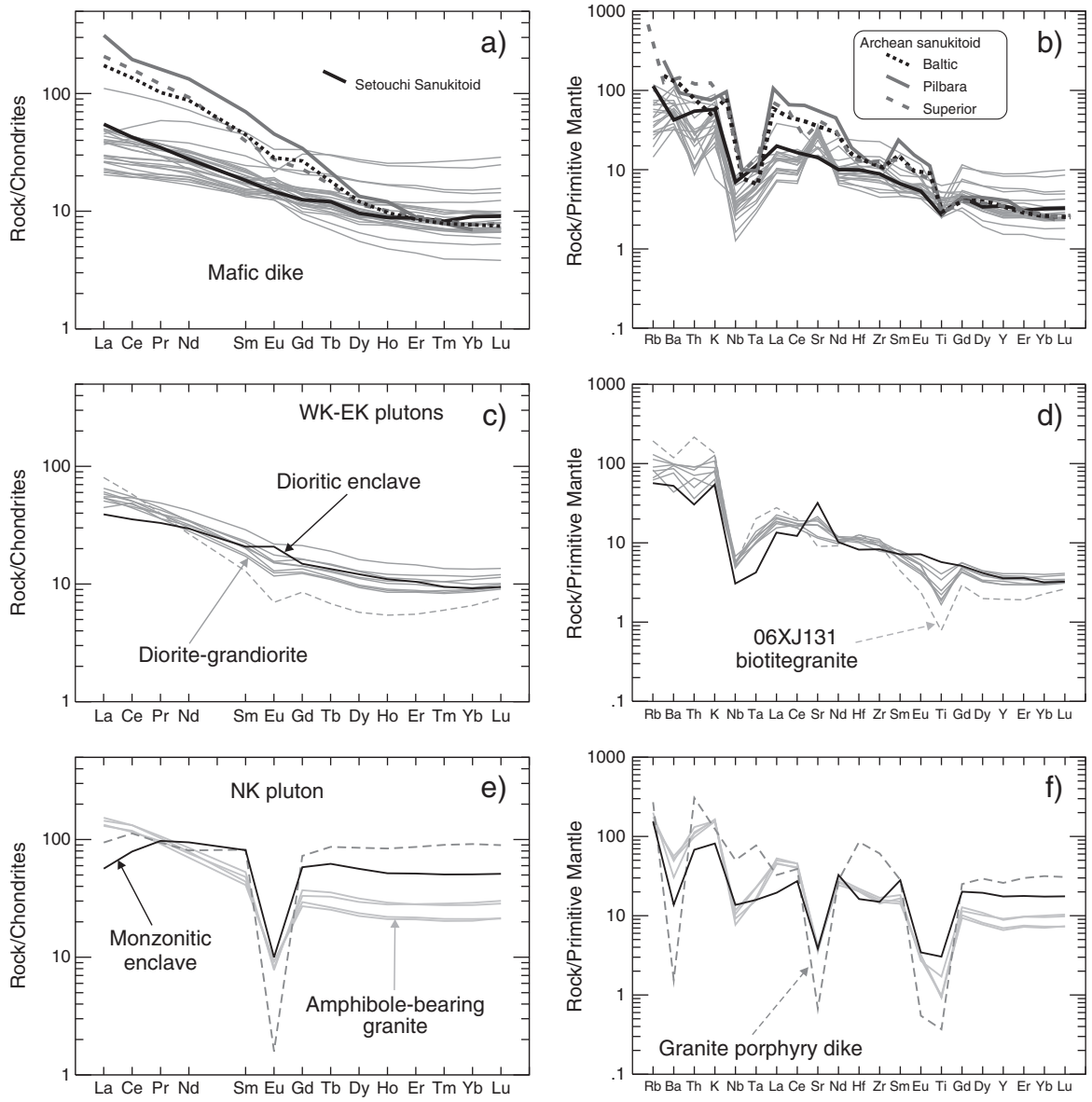


**Fig. 9.** Chondrite-normalized rare earth element patterns and Primitive Mantle (PM) normalized trace element diagrams for mafic dike (a and b), EK and WK plutons and mafic enclave (c and d), NK pluton and monzonitic enclave and granitic dike (e and f). Miocene sanukitoids from the Setouchi volcanic belt (Japan) (Shimoda et al., 1998; Tatsumi et al., 2003) are shown for comparison.
The chondrite and PM values are from Sun and McDonough (1989).

The diorites and granodiorites have slightly variable ranges for initial $^{87}Sr/^{86}Sr$ (0.7031–0.7049) and $^{143}Nd/^{144}Nd$ (0.51259–0.51269) ratios, with $\varepsilon_{Nd}(t)$ values varying from +6.8 to +8.7. The granodiorite-hosted dioritic enclave has higher initial $^{143}Nd/^{144}Nd$ (0.51269) ratios, with $\varepsilon_{Nd}(t)$ values of +8.7. The mafic dikes have similar initial $^{87}Sr/^{86}Sr$ and $^{143}Nd/^{144}Nd$ of 0.7035–0.7038 (except for one sample of 0.7048) and 0.51262–0.51269, with $\varepsilon_{Nd}(t)$ values of +7.3 to +8.7. The monzonitic enclave in the NK pluton and its host Am-bearing granites are characterized by slightly higher initial $^{87}Sr/^{86}Sr$ (0.7043–0.7047) and by $^{143}Nd/^{144}Nd$ (0.51265–0.51268) ratios corresponding to $\varepsilon_{Nd}(t)$ of +7.9 to +8.5. The granitic porphyry dike has an extremely high $^{87}Rb/^{86}Sr$ ratio of 34.35 and, as a result, the initial $^{87}Sr/^{86}Sr$ value cannot be used in determining magma petrogenesis (Jahn et al., 2000; Wu et al., 2002). It also has a high initial $^{143}Nd/^{144}Nd$ ratio of 0.51261 and $\varepsilon_{Nd}(t)$ value of +7.1. All the rocks have young Nd model ages ($T_{2DM}$) of 362–515 Ma (Fig. 10).

### 3.3.3. Zircon Hf isotope data

*In situ* zircon Hf isotope compositions from four samples are listed in Appendix 8 and shown on Fig. 10. Zircons from the diorites and granodiorites of WK (06XJ131) and EK (06XJ136, 06XJ182) plutons have variable Hf isotope compositions. Diorite zircon grains $^{176}Hf/^{177}Hf$ ratios ranging from 0.282861 to 0.283026 and $\varepsilon_{Hf}(t)$ values from +9.9 to +15.7. Zircon grains from granodiorite samples 06XJ136 and 06XJ182 have $^{176}Hf/^{177}Hf$ ratios ranging from 0.282858 to 0.283031 and from 0.282895 to 0.283021 and $\varepsilon_{Hf}(t)$ values from +9.8 to +15.9 and +11.1 to +15.2, respectively. Zircons from the mafic dike sample 06XJ134 have variable Hf isotope compositions with $^{176}Hf/^{177}Hf$ ratios ranging from 0.282913 to 0.283016 and $\varepsilon_{Hf}(t)$ values from 11.9 to 15.5. Zircon grains from the monzonitic enclave (06XJ121-2) in the NK pluton and its host Am-bearing granites (06XJ120) have similar and relatively homogeneous Hf isotope compositions with $^{176}Hf/^{177}Hf$ ratios 0.282921–0.283041

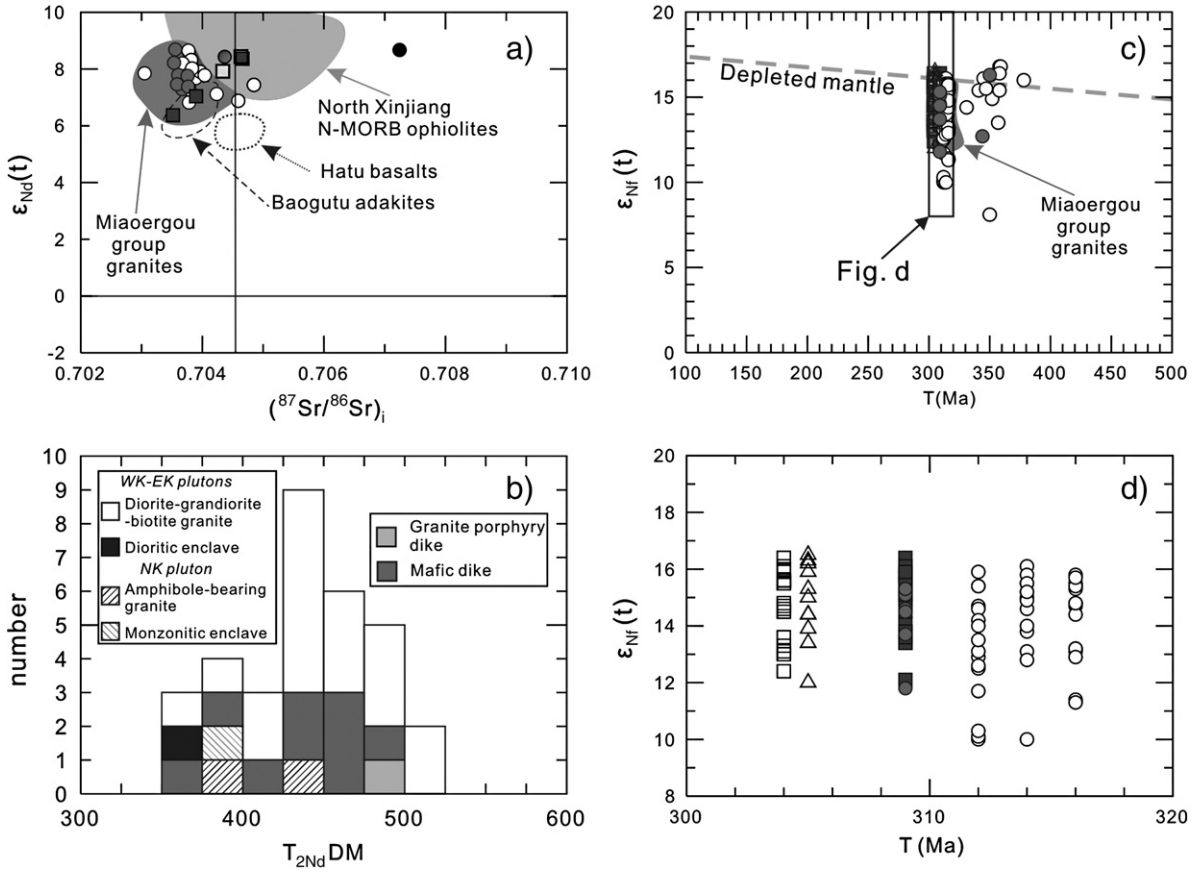


**Fig. 10.** (a) $\varepsilon_{Nd}(t)$ vs. $(^{87}Sr/^{86}Sr)_i$, (b) Nd model age histogram and diagram of T (Ma) − $\varepsilon_{Hf}(t)$ (c and d) for the granitoids, dikes and mafic enclaves in the Keramay area (western Junggar).
Data for the Baogutu adakites and Hatu basalts are from Tang et al. (2010; submitted for publication); data for the Miaoergou granites are from Chen and Arakawa (2005) and Geng et al. (2009). North Xinjiang ophiolite field is from Tang et al. (2012).

and 0.282934–0.283046, $\varepsilon_{Hf}(t)$ values of +12.0 to +16.3 and +12.4 to +16.4, respectively. Zircon grains from the granitic porphyry dike (06XJ123) also have homogeneous Hf isotope compositions with $^{176}Hf/^{177}Hf$ ratios ranging from 0.282922 to 0.283048 and $\varepsilon_{Hf}(t)$ values of +12.0 to +16.5, similar to those from the NK pluton.

## 4. Discussion

### 4.1. Physical–chemical conditions of emplacement

Magma crystallization temperatures can be calculated by zircon thermometry (Watson and Harrison, 1983). The zircon thermometer gives temperatures that vary between 619 and 788 °C (EK–WK plutons), 641 and 796 °C (mafic dikes), and 783 and 939 °C (NK pluton). The results suggest that the Am-bearing granites from the NK pluton have the highest zircon saturation temperature among these intrusive rocks.

Experimental studies have shown that the Fe/(Fe + Mg) ratio of mafic silicates and whole rocks is a function of $fO_2$ at fixed temperature (Anderson and Smith, 1995; Dall'agnol et al., 1999; Prouteau and Scaillet, 2003; Scaillet and Evans, 1999). The Fe/(Fe + Mg) ratios of amphiboles increase from mafic dikes and the EK–WK plutons towards the NK pluton (Fig. 11), the FeO/MgO ratios of whole rocks also show a similar trend, indicating the dikes formed at higher oxidizing conditions than the plutons. EK–WK plutons and related dioritic enclaves, mafic dikes have whole rock Fe/Mg ratios similar to those of the Pinatubo dacite (Luzon Island, Philippines) (Prouteau and Scaillet, 2003; Scaillet and Evans, 1999). Therefore, based on the empirical relationships derived from the Fe/(Fe + Mg) of amphibole and $fO_2$ (Prouteau and Scaillet, 2003; Scaillet and Evans, 1999), we may deduce the redox conditions for those rocks (Fig. 11). The results give a range between NNO + 0.6 and NNO + 1.8, NNO − 0.6 and NNO + 1.5, and NNO + 1.5 and NNO + 2.7, for EK–WK plutons and related dioritic enclaves, mafic dikes, respectively.

The $H_2O$ content, which depends on the temperature and pressure as well as melt compositions, can be estimated empirically from experimental data (Dall'agnol et al., 1999; Klimm et al., 2003; Prouteau and Scaillet, 2003; Scaillet and Evans, 1999). The stability of amphibole is extremely dependent on the $H_2O$ content of the melt (Scaillet and Evans, 1999). Based on available experimental results (Scaillet and Evans, 1999), the stability of amphiboles and the absence of orthopyroxenes in EK–WK plutons, related diorite enclaves, and mafic dikes suggests water content > 5 wt.%. The amphibole-bearing granites from the NK pluton show A-type granite characteristics and are geochemically similar to metaluminous A-type granites from Lachlan Fold Belt. Klimm et al. (2003) estimated that initial water contents in the Lachlan Fold Belt A-type granite melts were between 2 and 3 wt.% $H_2O$ and the NK pluton magma may have had similar $H_2O$ contents.

### 4.2. Mafic dike: partial melting of metasomatized mantle

Compositionally, the most mafic dike samples from the central western Junggar region (Figs. 7, 8 and 12) are broadly similar to those of Cenozoic arc high-Mg andesite (sanukitoid) in the Setouchi Volcanic Belt from southwestern Japan and the Archean sanukitoid

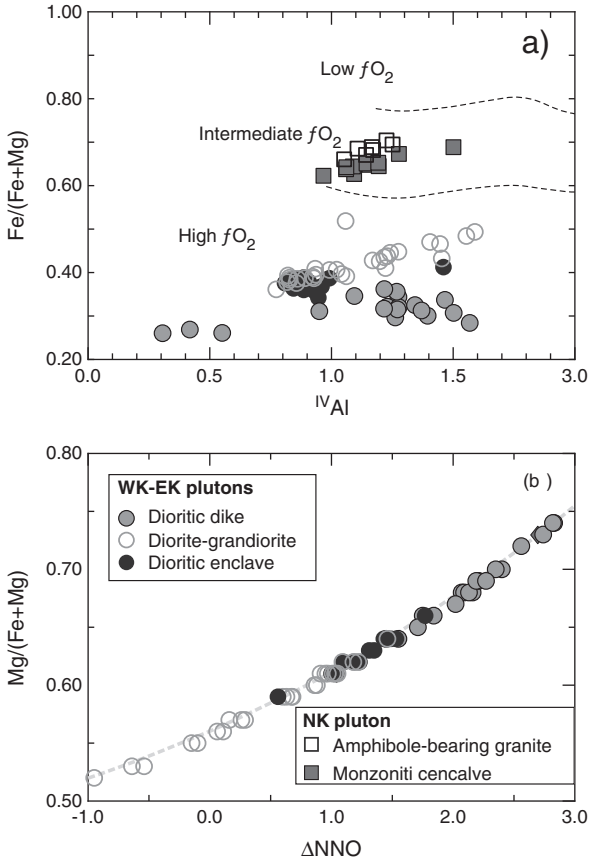


**Fig. 11.** (a) Amphibole Fe/(Fe + Mg) vs $^{IV}$Al diagrams (Anderson and Smith, 1995) showing the possible oxygen fugacity conditions during the crystallization of rocks from the western Junggar region. (b) Estimation of oxygen fugacity conditions following the data of Scaillet and Evans (1999). The diagram illustrates the effect of $fO_2$ on the Mg-number of experimental hornblende in S-free dacites at 780 °C and 220 MPa. The curve for hornblende in the S-free system is a second-order polynomial fit: $\Delta NNO = -20.206 + 51.56\ (Mg^{\#}) - 27.605\ (Mg^{\#})^2$ with a correlation coefficient $r^2 = 0.995$ (Scaillet and Evans, 1999).

suite, which generally contain $SiO_2$ of 60 wt.% (or less), MgO > 6 wt.%, $Mg^{\#} > 60$, Ni and Cr > 100 ppm, coupled with high LILE and LREE and LREE/HREE ratios (Shirey and Hanson, 1984; Stern et al., 1989; Tatsumi, 2006; Tatsumi and Ishizaka, 1982). In detail, however, the Keramay mafic dikes exhibit some distinct geochemical characteristics. For example, compared to Archean sanukitoids, the Keramay mafic dikes have lower abundances of LREEs and LILEs abundances and LREE/HREE ratios (Fig. 9). These mafic dykes also contain higher LILE abundances than those in Cenozoic sanukitoids of the Setouchi Volcanic Belt (Fig. 9). The mafic dikes in the central western Junggar region contain high Sr and low Y, with high Sr/Y ratios (43 ± 13) relative to the Setouchi sanukitoids.

In order to calculate the parental melt of the mafic dike, we computed the melt composition in equilibrium with clinopyroxenes (early crystallization minerals) using the method of Tiepolo and Tribuzio (2008). The estimated melt composition (Fig. 13) is characterized by LILE and LREE enrichment. A weak positive Sr and negative Nb and Ti anomalies are observed. Most trace elements show a similar pattern between the calculated melt composition in terms of clinopyroxene compositions from the Keramay mafic dikes and high-Mg andesite from the Setouchi Volcanic Belt (Shimoda et al., 1998; Tatsumi and Ishizaka, 1982; Tatsumi et al., 2003), indicating genetic affinities between the two igneous suites.

The high $Mg^{\#}$, Cr and Ni contents and low Th contents of these mafic dikes (Figs. 8 and 12), combined with the high Cr and $Mg^{\#}$ of their clinopyroxenes, distinguish the Keramay mafic dikes from any crustal materials (Rudnick and Gao, 2003) or crustally derived melts (Patiño Douce, 2005; Rapp and Watson, 1995), indicating a mantle source. In addition, they are enriched in LILEs and LREEs and depleted in HREEs and high field strength elements (HFSEs), with negative Nb, Ta, Ti and P anomalies (Fig. 9). Their $\varepsilon_{Nd}(t)$ and $\varepsilon_{Hf}(t)$ values are slightly less than those of the depleted mantle (Fig. 10). These geochemical features suggest that they were most likely derived from an enriched mantle source metasomatized by recycled crustal materials. Alternatively, they may have originated from a depleted mantle source but were contaminated by crustal materials en route during their ascent and emplacement. However, the mafic dikes have high and relatively homogeneous whole rock Nd and zircon Hf isotope compositions ($\varepsilon_{Nd}(t) = +7.3$ to $+8.7$; $\varepsilon_{Hf}(t) = +11.9$ to $+15.5$), contrary to what is expected from crustal assimilation, which would generally increase $SiO_2$ abundances and impart variable Nd–Hf isotopic compositions. The extremely young $T_{DM}$ values also suggest that the Keramay mafic magmas did not undergo significant contamination involving older continental crust. Thus, the geochemical and isotopic characteristics of the mafic dikes were inherited from their mantle source rather than by crustal assimilation. Therefore, these geochemical features are most plausibly attributed to a subduction-modified source, similar to those of other sanukitoids (Heilimo et al., 2010; Martin et al., 2009; Shirey and Hanson, 1984; Stern et al., 1989; Whalen et al., 2004).

Based on their geochemical and isotopic characteristics, it has been suggested that individual sanukitoid suites originated from enriched mantle sources metasomatized by sediments (Shimoda et al., 1998; Tatsumi, 2006), slab-derived (adakitic) melts (Martin et al., 2005; Moyen et al., 2003; Rapp et al., 1999), or fluids dehydrated from the slab (Lobach-Zhuchenko et al., 2008). Sanukitoids associated with mantle sources enriched by subducted sediments, such as those of the Setouchi Volcanic Belt, SW Japan, have low Sr/Y (19.8 ± 4.8) and Sr/Ce (10.4 ± 2.7) ratios and high Th/La (0.35 ± 0.09) (Shimoda et al., 1998; Tatsumi et al., 2006). However, the western Junggar mafic dikes exhibit higher Sr/Y (43 ± 13) and Sr/Ce (33 ± 13) ratios, and $\varepsilon_{Nd}(t)$ and $\varepsilon_{Hf}(t)$ values, and lower Th/La (0.19 ± 0.04) that cannot be attributed to a mantle source modified mainly by subducted sediments. It is generally accepted that Zr and Hf typically display significant mobility in slab melts but low solubility in fluids (e.g., La Flèche et al., 1998). Consequently, the enrichment of Zr and Hf relative to Nd and Sm is characteristic of magmas derived from a mantle source metasomatized by subduction-related melts and minor fluids and we infer such an origin for the western Junggar Keramay sanukitoid dikes (Fig. 12).

It is important to note the geochemical and isotopic similarities and differences between the Keramay mafic dikes and the nearby and contemporaneous Baogutu adakites (Figs. 1, 7–9, 12). The Baogutu adakites were interpreted to have been produced by partial melting of subducted oceanic crust, and subsequent interactions between slab melts and mantle peridotite during their ascent (Tang et al., 2010). The Keramay mafic dikes can readily be distinguished by their higher compatible element contents, such as Cr and Ni, relative to the Baogutu adakites (Fig. 12). Clinopyroxenes of the Keramay mafic dikes have higher $Mg^{\#}$ values and MgO contents than those of the Baogutu adakites but are similar to the rims of clinopyroxenes in the adakites (Fig. 14). In addition, clinopyroxenes in the Keramay mafic dikes do not show reverse zoning, in contrast to those in the Baogutu adakites. The petrological evidence suggests that the Baogutu adakitic magmas originated from a low Mg source but assimilated a high Mg mantle component. Therefore, the Keramay mafic dikes and the Baogutu adakites most likely originated from an enriched mantle source and subducted oceanic crust, respectively. The enriched mantle source of the Keramay mafic dikes is likely to have been metasomatized by subducted oceanic crust-derived slab melts whereas the originally pure slab melts of the Baogutu adakites were hybridized by mantle

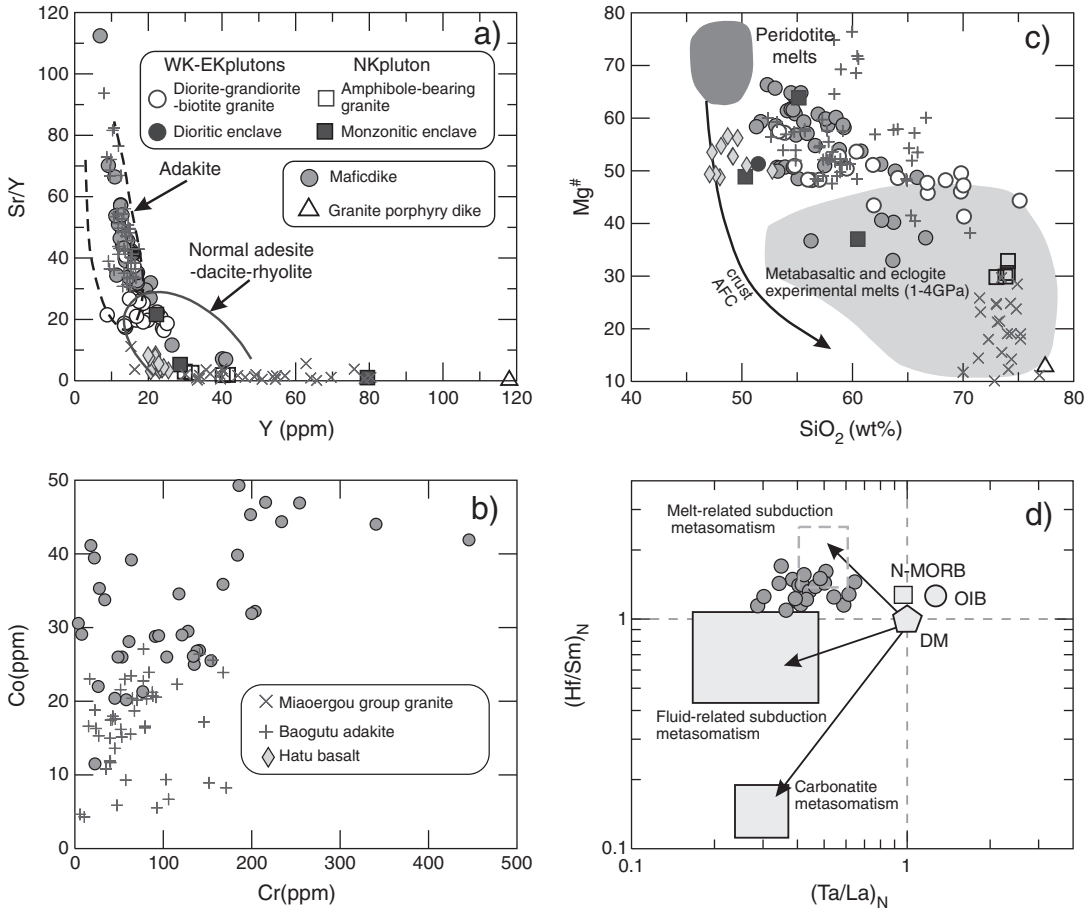


**Fig. 12.** (a) Sr/Y vs. Y and (b) Cr vs. Co diagrams. (c) $Mg^{\#}$ vs. $SiO_2$ and (d) $(Ta/La)_N$ vs. $(Hf/Sm)_N$ (after La Flèche et al., 1998). Data for the metabasaltic and eclogite experimental melts (1–4.0 GPa) in subpanel c are from Rapp and Watson (1995), Rapp et al. (1999), Sen and Dunn (1994).

peridotite during their ascent (Tang et al., 2010). Consequently, the two rock types share some whole rock geochemical characteristics.

### 4.3. Diorites and granodiorites: magma mixing

The diorites, granodiorites and biotite granites in the EK–WK plutons show a wide range of silica abundances ($SiO_2$ = 53.36–75.12 wt.%) combined with relatively high $Mg^{\#}$s (41–58) (Fig. 12c). They have slightly variable initial $^{87}Sr/^{87}Sr$ (0.7031–0.7049), $\varepsilon_{Nd}(t) = +6.8$ to $+8.7$) and zircon $\varepsilon_{Hf}(t)$ ($+9.9$ to $+15.9$) values (Fig. 10), precluding a simple evolution via closed-system fractionation processes, since such mechanisms cannot reproduce the variable isotope compositions (Yang et al., 2007b). The range of geochemical characteristics can be achieved by partial melting of the mafic lower crust (Rapp and Watson, 1995; Sen and Dunn, 1994; Wolf and Wyllie, 1994) or mixing between mantle- and crust-derived magmas (Barbarin, 2005; Karsli et al., 2007; Yang et al., 2007a, 2007b), followed by fractional crystallization, with or without crustal contamination.

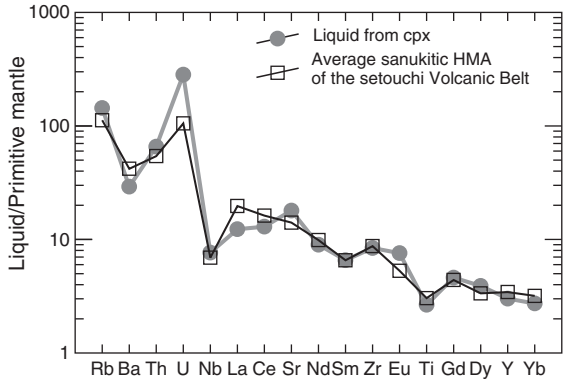


**Fig. 13.** Primitive mantle-normalized incompatible element pattern of the melt compositions calculated by using the average clinopyroxene composition from the mafic dike, compared to Cenozoic arc high-Mg andesite (sanukitoid) in the Setouchi volcanic belt from southwestern Japan (Shimoda et al., 1998; Tatsumi and Ishizaka, 1982; Tatsumi et al., 2003).

Partial melting of the mafic lower crust could produce metaluminous granitic magmas regardless of the degree of partial melting (Rapp and Watson, 1995; Sen and Dunn, 1994; Wolf and Wyllie, 1994). The felsic end member of the EK–WK plutons has higher $SiO_2$ of 75.12 wt.%, with low MgO of 0.34 wt.% and $Mg^{\#}$ of 44, consistent with those of melts derived by partial melting of the mafic lower crust (Fig. 12). The geochemical features, such as moderately fractionated REE, lack of Eu anomalies, and relatively high Sr and Ba contents (Fig. 9), indicate that their parental melts originated from partial melting of a lower crustal source at relatively high pressures with major amphibole and minor garnet, but without plagioclase, in the residue (Sen and Dunn, 1994), which implies that garnet-bearing amphibolite may have been the source rock. However, the diorites establish the existence of a second distinct source. Some of them are characterized by low $SiO_2$ abundance (53.36 wt.%), and high MgO (up to 5.81 wt.%) and $Mg^{\#}$s (up to 58) (Fig. 12), which is inconsistent with partial melting of the mafic lower crustal rocks and requires a mantle-derived component.

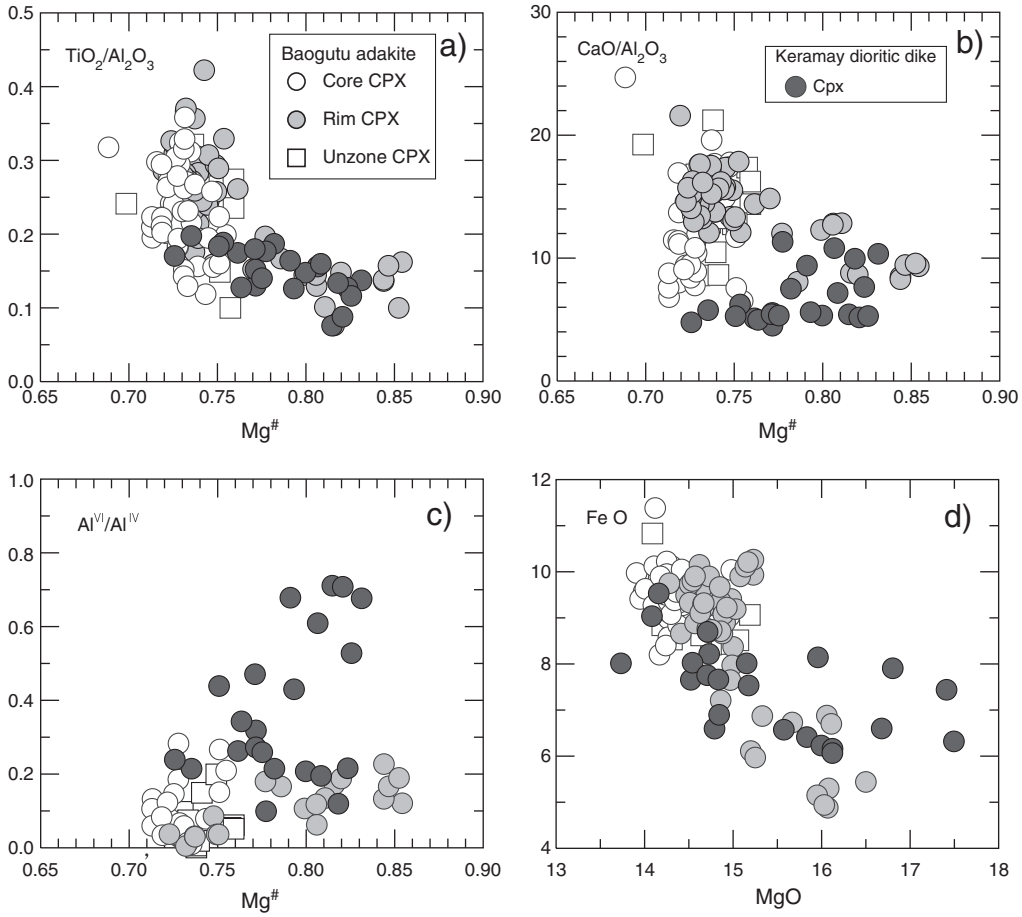


**Fig. 14.** Clinopyroxene compositions of the Keramay mafic dikes compared to those from the Baogutu adakites. Data for Baogutu adakite clinopyroxene compositions are from Tang et al.(2010).

Therefore, we suggest that the diorites and granodiorites in the EK–WK plutons were derived from the mixing between mantle- and crust-derived magmas. The dioritic enclaves in the EK–WK plutons establish a genetic link between the diorite dikes and the granodiorites. The diorite enclaves exhibit a fine grain size, and do not show a cumulate texture, in contrast to cumulates (Barbarin and Didier, 1992). The diorite enclaves contain no mineral formed by mica dehydration or cordierite, garnet, andalusite and sillimanite, and show igneous textures, which is in consistent with an origin as a residue (Chappell et al., 1987). The elliptical to round shapes of the dioritic enclaves and the occurrence of both rounded and diffuse contact zones between enclaves and host granites, suggest that they were plastic or entered the host magmas in a liquid state. Some of the dioritic enclaves contain large, rounded K-feldspar and quartz phenocrysts, which have sizes and compositions similar to those of the host granodiorites, indicating a transfer of mineral grains from the host magmas to the mafic enclave magma during mixing/mingling events (Vernon, 1984).

Some dioritic enclaves are characterized by the appearance of acicular apatite and larger acicular amphibole, which can be attributed to rapid cooling in a quenched magma, resulting from the mingling of small volumes of hot mafic magma with a cooler granitic melt (Barbarin, 2005; Bonin, 2004; Yang et al., 2006). Disequilibrium textures such as sieve and oscillatory plagioclases in the host granitoids also indicate magma mixing. Geochemically, the concentration of most major and trace elements show a near linear trend on diagrams against MgO (Fig. 8) consistent with a magma mixing of mafic and felsic magmas in various proportions. The host granitoids have a wider range of Sr–Nd–Hf isotope compositions and the sampled diorite enclave has a slightly higher $\varepsilon_{Nd}(t)$ value than those of the host (Fig. 10), indicating that two distinct components were involved. Ratio–ratio plots show definite hyperbolic arrays (e.g., Ti/Zr vs. Rb/Sr; Fig. 15), which is evidence for an interaction process involving at least two distinct compositional end-member magmas (Hollanda et al., 2003). The binary diagram of $^{143}Nd/^{144}Nd$ vs. $^{147}Sm/^{144}Nd$ (Fig. 15) confirms that the magma interaction process played an important role in the genesis of the granitoids from the EK–WK plutons.

The dioritic enclave has low $SiO_2$ (51.48 wt.%) and relative high $Mg^{\#}$ (52), enriched in LILEs (Sr = 673 ppm) and LREEs and depleted in HFSEs, with positive Eu and negative Nb, Ta, Ti and P anomalies (Fig. 9c–d). It has a whole rock $\varepsilon_{Nd}(t)$ value of +8.7 and a Nd model age of 363 Ma. All these geochemical features are similar to those of the contemporaneous spatially associated sanukitoid-type diorite dikes, implying that both originated from the same type of enriched lithospheric metasomatized mantle.

In addition to magma mixing, fractional crystallization could also have played a significant role in generating the diversity of rock types in the EK–WK plutons. The $Al_2O_3$, FeO and CaO contents decrease with decreasing MgO content, as do V, Cr and Ni (Fig. 8). The $CaO/Al_2O_3$ vs. MgO and CaO vs. MgO trends both steepen with declining MgO contents. Collectively, these relationships are consistent with the continuous fractionation of pyroxene. This scenario is supported by trace element modeling (Fig. 15c) where the trend for the diorites and granodiorites on a Cr–Ni diagram implies the fractionation of clinopyroxene and minor amounts of olivine. The abundance of Ba increases whereas Sr decreases with decreasing MgO (Fig. 8),

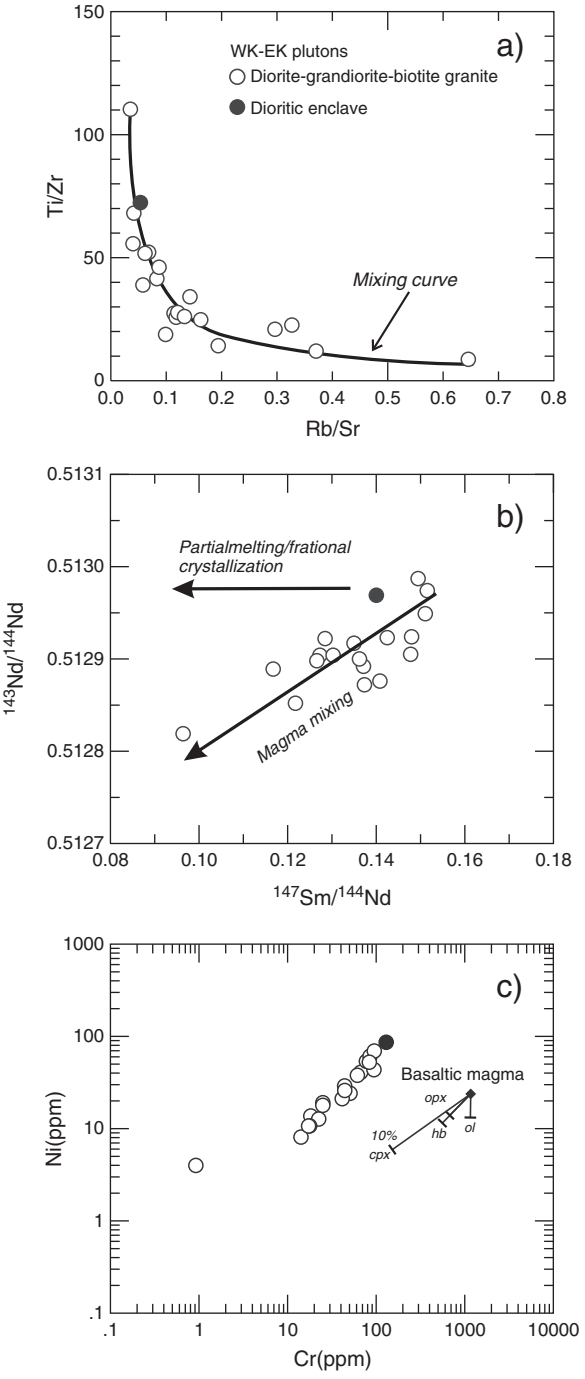


**Fig. 15.** (a) Ti/Zr vs. Rb/Sr, (b) $^{143}Nd/^{144}Nd$ vs. $^{147}Sm/^{144}Nd$ (c) Cr vs. Ni diagram showing the magma mixing and fractional crystallization for EK and WK plutons and dioritic enclave from the western Junggar region, southwestern CAOB. Fig. 15c illustrates clinopyroxene dominated fractionation.
Partition coefficients are from Rollinson (1993).

suggesting that feldspar is not a major fractionated phase, which is consistent with the negligible negative Eu anomalies in these rocks (Fig. 9). With decreasing MgO contents, the decrease of $TiO_2$ may be related to titanite and magnetite fractionation, consistent with the range of negative Ti anomalies on multi-element plots (Figs. 8–9) and the observed accessory mineral phases. Accordingly, fractional crystallization clearly contributed to the range of chemical compositions observed in the plutons.

### 4.4. Am-bearing granites and granite porphyry dike: partial melting of a juvenile crustal source

The Am-bearing granites of the NK pluton and nearby granite porphyry dike are geochemically similar to A-type granites (Eby, 1990; 1992; Whalen et al., 1987) (Figs. 7–9 and 16). The F and Cl contents of biotites in the granites reflect the nature of their parental host magmas. The original F contents in the melt ($F_{melt}$) can be calculated on the basis of the biotite Mg/(Mg + Fe + Mn) ratios (Mg index.) and the correlation with the F partition coefficient between melt and biotite found experimentally by Icenhower and London (1997). Based on this method, the estimated $F_{melt}$ contents vary from 3107 to 4710 ppm for the Am-bearing granites of the NK pluton and its monzonitic enclave, similar to the western Argentina $A_2$ granites and A-type granites in general (F = 580–5600 ppm) (Dahlquist et al., 2010). In contrast, diorites and granodiorites from the EK–WK plutons are characterized by extremely low $F_{melt}$ contents ranging from 83 to 379 ppm (Fig. 16), indicating that the NK-plutons have a distinct petrogenesis from the magma mixing model proposed for the diorites and EK–WK granodiorite plutons.

The Am-bearing granites of the NK pluton are characterized by highly radiogenic whole rock $\varepsilon_{Nd}(t)$ (+7.12 to +8.44) and zircon $\varepsilon_{Hf}(t)$ (+12 to +16.5) values with young Nd model (0.38–0.49 Ga) and Hf model (0.30–0.45 Ga) ages. They have higher $\varepsilon_{Nd}(t)$ values than those of slightly older (~315 Ma) Hatu basalts (Fig. 10), indicating they could not have been generated by fractional crystallization, magma mixing or crustal contamination involving the basalts (Tang et al., submitted for publication). Their extremely depleted isotope compositions indicate that only a recycled oceanic crustal component, represented by the lavas in the Cambrian–Carboniferous North Xinjiang ophiolites, is an appropriate magma source for the NK pluton (Tang et al., 2012). The NK pluton granites are characterized by strongly negative Eu and Sr anomalies on the chondrite REE and PM-normalized trace element patterns (Fig. 9), indicating that plagioclase remained in the source residue or was fractionated during magmatic evolution. In addition, they have high concentrations of HREE (Yb = 3.46–15.6 ppm; Y = 29.9–118 ppm) with low $(La/Yb)_N$ ratios of 1.0–7.3, precluding garnet in the residue. Thus, the Am-bearing granites in the NK pluton and granite porphyry dike most likely formed by partial melting of juvenile underthrusted or subducted oceanic crustal source at low pressure (<15 kbar) (e.g., Skjerlie and Patino Douce, 2002).

Detailed petrological observations suggest that rare monzonitic enclaves in the NK pluton are neither cumulates nor restites (Chappell et al., 1987). The sampled monzonitic enclave shows medium $SiO_2$ content of 60.48 wt.% and an $Mg^{\#}$ of 37. It is characterized by strongly negative Eu and Sr anomalies on chondrite-normalized REE and PM-normalized trace element patterns (Fig. 9), similar to its host Am-bearing granites. It also has a Nd–Hf isotope composition similar to the host rocks (Fig. 10, Appendices 7–8). Significantly negative Eu, Sr, P and Ti anomalies indicate the fractionation of plagioclase-, apatite- and Ti-bearing phases. Compared to the host granites, the monzonitic enclave has a lower La/Ce ratio and is enriched in HREEs and transition elements (e.g. Cr, Co, Ni, V), indicating that it contains more amphibole.

### 4.5. Geodynamic processes and implications for crustal growth in the CAOB

Zircon U–Pb dating indicates that mafic dikes, diorites, granodiorites, biotite granites, Am-bearing granites, granitic porphyry dikes, dioritic and monzonitic enclaves in the central western Junggar of the CAOB were generated in the Late Carboniferous (316–304 Ma). These rocks can be divided into three groups based on the geochemical characteristics: mafic dikes with sanukitoid features; diorites, granodiorites, biotite granites and dioritic enclaves; and Am-bearing

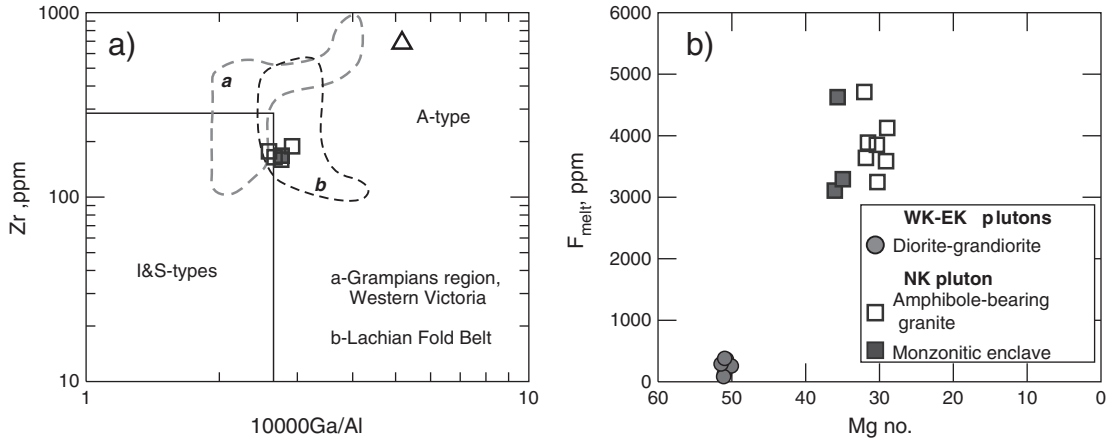


**Fig. 16.** (a) A-type granite discrimination diagrams (Whalen et al., 1987). (b) Plot of Mg# vs. F contents.

granites, their monozonitic enclaves and granite porphyry dikes. All of these rocks from western Junggar have strongly positive whole rock $\varepsilon_{Nd}(t)$ and zircon $\varepsilon_{Hf}(t)$ values with model ages less than 600 Ma, and have similar compositions and model ages to the vast expanse of granitoids in other areas of the CAOB such as: a) ca. 300 Ma granitoids from the eastern Junggar (Guo et al., 2010; Tang et al., 2008); b) Late Devonian–Early Permian A-type granites in the southern Altay Range (Shen et al., 2011); or c) Paleozoic granitoids in Kazakhstan (Heinhorst et al., 2000; Kröner et al., 2008). The depleted isotope compositions and young model ages of these granitoids indicate their derivation from juvenile sources and significant CAOB crustal growth during the time of their emplacement (Jahn, 2004; Jahn et al., 2000, 2004; Kröner et al., 2008; Wu et al., 2000, 2002).

Petrogenetic models for the genesis of Late Carbonifeous magmatic rocks in the Keramay area should account for their strongly positive $\varepsilon_{Nd}(t)$–$\varepsilon_{Hf}(t)$ isotope compositions, the subduction-related enrichment components in the mantle source, and the heat source for partial melting of mantle and crustal sources. They also need to account for both the elevated oxygen fugacity and wet character of magmas that formed the mafic dikes and granitoids of the EK–WK plutons while also explaining the low oxygen fugacity, high-F contents and low-$H_2O$ character of the magmas responsible for granites of the NK-pluton. In addition, the geodynamic scenario must be consistent with the presence of the contemporary Baogutu slab-derived adakites (315–310 Ma, Tang et al., 2010) and the Hatu "MORB-type" basalts (315 Ma, Tang et al., submitted for publication) in the Keramay region (western Junggar).

Many researchers have ascribed the melting of metasomatized mantle and related sanukitoid formation to a slab breakoff mechanism (Halla et al., 2009; Heilimo et al., 2010; Lobach-Zhuchenko et al., 2008; Whalen et al., 2004). In this study, the break-off model is not favored because (1) the distribution of Late Carboniferous granitoids in the western Junggar region (Fig. 1b) is inconsistent with slab breakoff, which predicts a narrow, linear zone of magmatism generally parallel to the subduction zone (Chung et al., 2005; Davies and von Blanckenburg, 1995; Xu et al., 2008); and (2) slab break-off is commonly triggered by attempted continental subduction (Chung et al., 2005; Davies and von Blanckenburg, 1995). However, there is no evidence for ancient continental blocks in the Junggar region (Hu et al., 2000; Sun et al., 2008), or evidence for continental subduction or collision in this area. The young model Nd and Hf ages of these rocks also suggest that there is insignificant ancient continent material involvement in their genesis.

An alternative model for the formation of both the adakitic rocks and the Am-bearing granites in the western Junggar region invokes ridge subduction and a resultant slab window, as proposed by Liu et al. (2007), Geng et al. (2009) and Tang et al.(2010). In this model the Junggar oceanic plate likely subducted beneath the western Junggar region creating the Keramay intra-oceanic arc in the Early Carboniferous (Geng et al., 2009, 2011; Tang et al., 2010, 2012, submitted for publication; Yin et al., 2010). At ca. 320 Ma, spreading center subduction began and resulted in a slab window (Thorkelson, 1996) that induced upwelling of asthenospheric mantle and creation of a "blowtorch effect" (DeLong et al., 1979). In this scenario, (1) melting of the subducted slab edge generated the Baogutu adakites (Tang et al., 2010); (2) melts/fluids released from the subducted slab metasomatised the lithospheric mantle, creating an enriched mantle source; (3) continued upwelling of asthenospheric mantle provided the thermal flux that induced partial melting of shallow crustal sources and the metasomatized mantle resulting in the generation of A-type granite magmas of the NK pluton and the sanukitoid magmas represented by the mafic dikes, respectively, and (4) mixing between these mantle- and lower crust-derived magmas produced diorites and granodiorites of the EK–WK plutons.

## 5. Conclusions

Zircon U–Pb ages of mafic dikes, granitoids, dioritic–monzonitic enclaves and granite porphyry dike from the western Junggar region in southwestern part of the CAOB indicate that these intrusions were emplaced at 316–304 Ma. Field observations, mineralogical, geochemical, whole rock Sr–Nd and zircon Hf isotopic data suggest that the sanukitoid mafic dikes were derived by partial melting of an enriched lithospheric mantle source. The diorites and granodiorites were produced by mixing between mantle-derived mafic and lower recycled oceanic crust-derived felsic magmas, coupled with minor fractional crystallization. The Am-bearing granites and granitic dike were generated by partial melting of juvenile crustal materials at a shallow crustal level. The widespread Late Carboniferous magmatism in the western Junggar region of southwestern CAOB was related to ridge subduction and a resultant slab window, which played an important role in the crustal growth for the CAOB.

Supplementary materials related to this article can be found online at doi:10.1016/j.lithos.2012.01.025.

## Acknowledgements

We would like to thank Editor-in-Chief Dr. Andrew Kerr and two anonymous reviewers for their constructive and helpful reviews. We appreciate the assistance of Jin-Hui Yang, Liewei Xie, Ying Liu, Guangqian Hu, Jinlong Ma, Xirong Liang and Xianglin Tu for geochemical analyses. This study was jointly supported by the Major

State Basic Research Program (973 Program) of People's Republic of China (nos. 2010CB808906 and 2007CB411308) and the National Natural Science Foundation of China (grants nos. 41025006, 41073029 and 41121002). This is contribution No. IS-1448 from GIGCAS.

## References


Abdel Rahman, A.M., 1994. Nature of biotites from alkaline, calc-alkaline, and peraluminous magmas. Journal of Petrology 35 (2), 525–541.

Albarède, F., 1998. The growth of continental crust. Tectonophysics 296 (1–2), 1–14.

Anderson, J.L., Smith, D.R., 1995. The effects of temperature and $fO_2$ on the Al-in-hornblende barometer. American Mineralogist 80 (5–6), 549–559.

Barbarin, B., 2005. Mafic magmatic enclaves and mafic rocks associated with some granitoids of the central Sierra Nevada batholith, California: nature, origin, and relations with the hosts. Lithos 80 (1–4), 155–177.

Barbarin, B., Didier, J., 1992. Genesis and evolution of mafic microgranular enclaves through various types of interaction between coexisting felsic and mafic magmas. Transactions of the Royal Society of Edinburgh Earth Science 83, 145–153.

Belousova, E., Griffin, W., O'Reilly, S.Y., Fisher, N., 2002. Igneous zircon: trace element composition as an indicator of source rock type. Contributions to Mineralogy and Petrology 143 (5), 602–622.

Bonin, B., 2004. Do coeval mafic and felsic magmas in post-collisional to within-plate regimes necessarily imply two contrasting, mantle and crustal, sources? A review. Lithos 78 (1–2), 1–24.

Chappell, B.W., White, A.J.R., Wyborn, D., 1987. The importance of residual source material (restite) in granite petrogenesis. Journal of Petrology 28 (6), 1111–1138.

Chen, B., Arakawa, Y., 2005. Elemental and Nd–Sr isotopic geochemistry of granitoids from the West Junggar foldbelt (NW China), with implications for Phanerozoic continental growth. Geochimica et Cosmochimica Acta 69 (5), 1307–1320.

Chen, B., Jahn, B.M., 2004. Genesis of post-collisional granitoids and basement nature of the Junggar Terrane, NW China: Nd–Sr isotope and trace element evidence. Journal of Asian Earth Science 23 (5), 691–703.

Chung, S.L., Chu, M.F., Zhang, Y.Q., Xie, Y.W., Lo, C.H., Lee, T.Y., Lan, C.Y., Li, X.H., Zhang, Q., Wang, Y.Z., 2005. Tibetan tectonic evolution inferred from spatial and temporal variations in post-collisional magmatism. Earth-Science Reviews 68 (3–4), 173–196.

Condie, K.C., 2000. Episodic continental growth models: afterthoughts and extensions. Tectonophysics 322 (1–2), 153–162.

Dahlquist, J.A., Alasino, P.H., Eby, G.N., Galindo, C., Casquet, C., 2010. Fault controlled Carboniferous A-type magmatism in the proto-Andean foreland (Sierras Pampeanas, Argentina): geochemical constraints and petrogenesis. Lithos 115 (1–4), 65–81.

Dall'agnol, R., Scaillet, B., Pichavant, M., 1999. An experimental study of a lower proterozoic A-type granite from the eastern Amazonian Craton, Brazil. Journal of Petrology 40 (11), 1673–1698.

Davidson, J.P., Arculus, R.J., 2006. The significance of Phanerozoic arc magmatism in generating continental crust. In: Brown, M., Rushmer, T. (Eds.), Evolution and Differentiation of the Continental Crust. Cambridge University Press, pp. 135–172.

Davies, J.H., von Blanckenburg, F., 1995. Slab breakoff: a model of lithosphere detachment and its test in the magmatism and deformation of collisional orogens. Earth and Planetary Science Letters 129 (1–4), 85–102.

DeLong, S.E., Schwarz, W.M., Anderson, R.N., 1979. Thermal effects of ridge subduction. Earth and Planetary Science Letters 44 (2), 239–246.

Eby, G.N., 1990. The A-type granitoids: a review of their occurrence and chemical characteristics and speculations on their petrogenesis. Lithos 26 (1–2), 115–134.

Eby, G.N., 1992. Chemical subdivision of the A-type granitoids: petrogenetic and tectonic implications. Geology 20 (7), 641–644.

Foster, M., 1960. Interpretation of the composition of trioctahedral micas. U.S. Geological Survey Professional Paper 354, 11–49.

Frost, C.D., Bell, J.M., Frost, B.R., Chamberlain, K.R., 2001. Crustal growth by magmatic underplating: isotopic evidence from the northern Sherman batholith. Geology 29 (6), 515–518.

Geng, H., Sun, M., Yuan, C., Xiao, W., Xian, W., Zhao, G., Zhang, L., Wong, K., Wu, F., 2009. Geochemical, Sr–Nd and zircon U–Pb–Hf isotopic studies of Late Carboniferous magmatism in the West Junggar, Xinjiang: implications for ridge subduction? Chemical Geology 266 (3–4), 364–389.

Geng, H.Y., Sun, M., Yunan, C., Zhao, G.C., Xiao, W.J., 2011. Geochemical and geochronological study of early Carboniferous volcanic rocks from the West Junggar: petrogeneses and tectonic implications. Journal of Asian Earth Science 42 (5), 854–866.

Guo, F.F., Jiang, C.Y., Lu, R.H., Xia, Z.D., Ling, J.L., Guo, N.X., 2010. Petrogenesis of the Huangyangshan alkali granites in Kalamaili area, northern Xinjiang. Acta Petrologica Sinica 26 (8), 2357–2373 (in Chinese with English abstract).

Halla, J., van Hunen, J., Heilimo, E., Hölttä, P., 2009. Geochemical and numerical constraints on Neoarchean plate tectonics. Precambrian Research 174 (1–2), 155–162.

Hawkesworth, C.J., Kemp, A.I.S., 2006. Evolution of the continental crust. Nature 443 (7113), 811–817.

Heilimo, E., Halla, J., Hölttä, P., 2010. Discrimination and origin of the sanukitoid series: geochemical constraints from the Neoarchean western Karelian Province (Finland). Lithos 115 (1–4), 27–39.

Heinhorst, J., Lehmann, B., Ermolov, P., Serykh, V., Zhurutin, S., 2000. Paleozoic crustal growth and metallogeny of Central Asia: evidence from magmatic–hydrothermal ore systems of Central Kazakhstan. Tectonophysics 328, 69–87.

Hollanda, M., Pimentel, M., Jardim de Sá, E., 2003. Paleoproterozoic subduction-related metasomatic signatures in the lithospheric mantle beneath NE Brazil: inferences from trace element and Sr–Nd–Pb isotopic compositions of Neoproterozoic high-K igneous rocks. Journal of South American Earth Science 15 (8), 885–900.

Hu, A.Q., Jahn, B.M., Zhang, G.X., Chen, Y.B., Zhang, Q.F., 2000. Crustal evolution and Phanerozoic crustal growth in northern Xinjiang: Nd isotopic evidence. Part I. Isotopic characterization of basement rocks. Tectonophysics 328 (1–2), 15–51.

Icenhower, J.P., London, D., 1997. Partitioning of fluorine and chlorine between biotite and granitic melt: experimental calibration at 200 MPa $H_2O$. Contributions to Mineralogy and Petrology 127 (1), 17–29.

Jahn, B.M., 2004. The Central Asian Orogenic Belt and growth of the continental crust in the Phanerozoic. In: Malpas, J., Fletcher, C.J.N., Ali, J.R., Aichison, J.C. (Eds.), Aspects of the Tectonic Evolution of China: Geological Society, London, Special Publication, pp. 73–100. London.

Jahn, B.M., Wu, F.Y., Chen, B., 2000. Massive granitoid generation in Central Asia: Ndisotope evidence and implication for continental growth in the Phanerozoic. Episodes 23 (2), 82–92.

Jahn, B.M., Capdevila, R., Liu, D., Vernon, A., Badarch, G., 2004. Sources of Phanerozoic granitoids in the transect Bayanhongor-Ulaan Baatar, Mongolia: geochemical and Nd isotopic evidence, and implications for Phanerozoic crustal growth. Journal of Asian Earth Science 23 (5), 629–653.

Jian, P., Liu, D.Y., Kroner, A., Windley, B.F., Shi, Y., Zhang, F., Shi, G., Miao, L., Zhang, W., Zhang, Q., Zhang, L., Ren, J., 2008. Time scale of an early to mid-Paleozoic orogenic cycle of the long-lived Central Asian Orogenic Belt, Inner Mongolia of China: implications for continental growth. Lithos 101, 233–259.

Karsli, O., Chen, B., Aydin, F., Sen, C., 2007. Geochemical and Sr–Nd–Pb isotopic compositions of the Eocene Dolek and Saricicek Plutons, Eastern Turkey: implications for magma interaction in the genesis of high-K calc-alkaline granitoids in a post-collision extensional setting. Lithos 98 (1–4), 67–96.

Kelemen, P.B., 1995. Genesis of high $Mg^{\#}$ andesites and the continental-crust. Contributions to Mineralogy and Petrology 120 (1), 1–19.

Kemp, A.I.S., Hawkesworth, C.J., Paterson, B.A., Kinny, P.D., 2006. Episodic growth of the Gondwana supercontinent from hafnium and oxygen isotopes in zircon. Nature 439 (7076), 580–583.

Kerr, A.C., Pearson, D.G., Nowell, G.M., 2009. Magma source evolution beneath the Caribbean oceanic plateau: new insights from elemental and Sr–Nd–Pb–Hf isotopic studies of ODP Leg 165 Site 1001 basalts. Geological Society of London. Special Publication 328 (1), 809–827.

Khain, E.V., Bibikova, E.V., Krˆner, A., Zhuravlev, D.Z., Sklyarov, E.V., Fedotova, A.A., Kravchenko-Berezhnoy, I.R., 2002. The most ancient ophiolite of the Central Asian fold belt: U–Pb and Pb–Pb zircon ages for the Dunzhugur Complex, Eastern Sayan, Siberia, and geodynamic implications. Earth and Planetary Science Letters 199 (3–4), 311–325.

Klimm, K., Holtz, F., Johannes, W., King, P.L., 2003. Fractionation of metaluminous A-type granites: an experimental study of the Wangrah Suite, Lachlan Fold Belt, Australia. Precambrian Research 124 (2–4), 327–341.

Koto, B., 1916. On the volcanoes of Japan (V). Journal Geological Society Tokyo 23, 95–127.

Kovalenko, V.I., Yarmolyuk, V.V., Kovach, V.P., Kotov, A.B., Kozakov, I.K., Salnikova, E.B., Larin, A.M., 2004. Isotope provinces, mechanisms of generation and sources of the continental crust in the Central Asian mobile belt: geological and isotopic evidence. Journal of Asian Earth Science 23 (5), 605–627.

Kröner, A., Hegner, E., Lehmann, B., Heinhorst, J., Wingate, M.T.D., Liu, D.Y., Ermelov, P., 2008. Palaeozoic arc magmatism in the Central Asian Orogenic Belt of Kazakhstan: SHRIMP zircon ages and whole-rock Nd isotopic systematics. Journal of Asian Earth Science 32 (2–4), 118–130.

La Flèche, M.R., Camiré, G., Jenner, G.A., 1998. Geochemistry of post-Acadian, Carboniferous continental intraplate basalts from the Maritimes Basin, Magdalen Islands, Quebec, Canada. Chemical Geology 148 (3–4), 115–136.

Lapierre, H., Bosch, D., Tardy, M., Struik, L.C., 2003. Late Paleozoic and Triassic plume-derived magmas in the Canadian Cordillera played a key role in continental crust growth. Chemical Geology 201 (1–2), 55–89.

Leake, B.E., Woolley, A.R., Arps, C.E.S., Birch, W.D., Gilbert, M.C., Grice, J.D., Hawthorne, F.C., Kato, A., Kisch, H.J., Krivovichev, V.G., Linthout, K., Laird, J., Mandarino, J.A., Maresch, W.V., Nickel, E.H., Rock, N.M.S., Schumacher, J.C., Smith, D.C., Stephenson, N.C.N., Ungaretti, L., Whittaker, E.J.W., Youzhi, Guo, 1997. Nomenclature of amphiboles; report of the Subcommittee on Amphiboles of the International Mineralogical Association, Commission on New Minerals and Mineral Names. American Mineralogist 82 (9–10), 1019–1037.

Li, X.Z., Han, B.F., Ji, J.Q., Li, Z.H., Liu, Z.Q., Yang, B., 2004. Geology, geochenistry and K-Ar ages of the Karamay basic-intermediate dyke swarm from Xinjiang, China. Geochimica 33, 574–584 (in Chinese with English abstract).

Liu, X.J., Xu, J.F., Hou, Q.Y., Bai, Z.H., Lei, M., 2007. Geochemical characteristics of Karamaili ophiolite in east Junggar, Xingjiang: products of ridge subduction. Xingjiang: products of ridge subduction. Acta Petrologica Sinica 23, 1591–1602 (in Chinese with English abstract).

Lobach-Zhuchenko, S.B., Rollinson, H., Chekulaev, V.P., Savatenkov, V.M., Kovalenko, A.V., Martin, H., Guseva, N.S., Arestova, N.A., 2008. Petrology of a late Archaean, highly potassic, sanukitoid pluton from the Baltic Shield: insights into late Archaean mantle metasomatism. Journal of Petrology 49 (3), 393–420.

Mann, P., Taira, A., 2004. Global tectonic significance of the Solomon Islands and Ontong Java Plateau convergent zone. Tectonophysics 389 (3–4), 137–190.

Martin, H., Smithies, R.H., Rapp, R., Moyen, J.F., Champion, D., 2005. An overview of adakite, tonalite–trondhjemite–granodiorite (TTG), and sanukitoid: relationships and some implications for crustal evolution. Lithos 79 (1–2), 1–24.

Martin, H., Moyen, J.-F., Rapp, R., 2009. The sanukitoid series: magmatism at the Archaean? Proterozoic transition. Earth and Environmental Science Transactions of the Royal Society of Edinburgh 100 (Special Issue 1–2), 15–33.

Morimoto, N., Fabries, J., Ferguson, A.K., Ginzburg, I.V., Ross, M., Seifert, F.A., Zussman, J., Aoki, K., Gottardi, G., 1988. Nomenclature of pyroxenes. American Mineralogist 73 (9–10), 1123–1133.
Moyen, J.F., Martin, H., Jayananda, M., Auvray, B., 2003. Late Archaean granites: a typology based on the Dharwar Craton (India). Precambrian Research 127 (1–3), 103–123.
Patiño Douce, A.E., 2005. Vapor-absent melting of tonalite at 15–32 kbar. Journal of Petrology 46 (2), 275–290.
Prouteau, G., Scaillet, B., 2003. Experimental constraints on the origin of the 1991 Pinatubo dacite. Journal of Petrology 44 (12), 2203–2241.
Rapp, R.P., Watson, E.B., 1995. Dehydration melting of metabasalt at 8–32 kbar: implications for continental growth and crust–mantle recycling. Journal of Petrology 36 (4), 891–931.
Rapp, R.P., Shimizu, N., Norman, M.D., Applegate, G.S., 1999. Reaction between slab-derived melts and peridotite in the mantle wedge: experimental constraints at 3.8 GPa. Chemical Geology 160 (4), 335–356.
Reymer, A., Schubert, G., 1986. Rapid growth of some major segments of continental crust. Geology 14 (4), 299–302.
Rieder, M., Cavazzini, G., D'yakonov, Y.S., Frank-Kamenetskii, V.A., Gottardi, G., Guggenheim, S., Koval, P.V., Mueller, G., Neiva, A.M.R., Radoslovich, E.W., Robert, J.-L., Sassi, F.P., Takeda, H., Weiss, Z., Wones, D.R., 1998. Nomenclature of the micas. Clay Clay Mineralogy 46 (5), 586–595.
Rollinson, H., 1993. Using Geochemical Data, 352 pp., Longman, London.
Rudnick, R.L., 1995. Making continental crust. Nature 378, 573–578.
Rudnick, R. L., Gao, S., 2003. The composition of the continental crust. In: Rudnick, R.L. (Ed.), The Crust. Elsevier–Pergamon, Oxford, pp. 1–64., in The Crust, edited by R. L. Rudnick, pp. 1–64, Elsevier–Pergamon, Oxford,.
Scaillet, B., Evans, B.W., 1999. The 15 June 1991 eruption of Mount Pinatubo. I. Phase equilibria and pre-eruption P–T–$fO_2$–$fH_2O$ conditions of the dacite magma. Journal of Petrology 40 (3), 381–411.
Sen, C., Dunn, T., 1994. Dehydration melting of a basaltic composition amphibolite at 1.5 and 2.0 GPa: implications for the origin of adakites. Contributions to Mineralogy and Petrology 117 (4), 394–409.
Sengör, A.M.C., Natal'in, B.A., Burtman, V.S., 1993. Evolution of the Altaid tectonic collage and Palaeozoic crustal growth in Eurasia. Nature 364 (6435), 299–307.
Shen, X., Zhang, H., Wang, Q., Wyman, D.A., Yang, Y., 2011. Late Devonian–Early Permian A-type granites in the southern Altay Range, Northwest China: petrogenesis and implications for tectonic setting of "A2-type" granites. Journal of Asian Earth Sciences 42, 986–1007.
Shimoda, G., Tatsumi, Y., Nohda, S., Ishizaka, K., Jahn, B.M., 1998. Setouchi high-Mg andesites revisited: geochemical evidence for melting of subducting sediments. Earth and Planetary Science Letters 160 (3–4), 479–492.
Shirey, S.B., Hanson, G.N., 1984. Mantle-derived Archean monzodiorites and trachyandesites. Nature 310, 222–224.
Skjerlie, K.P., Patino Douce, A.E., 2002. The fluid-absent partial melting of a zoisite-bearing quartz eclogite from 1.0 to 3.2 GPa; implications for melting in thickened continental crust and for subduction-zone processes. Journal of Petrology 43 (2), 291–314.
Smithies, R.H., Van Kranendonk, M.J., Champion, D.C., 2007. The Mesoarchean emergence of modern-style subduction. Gondwana Research 11 (1–2), 50–68.
Stern, R.A., Hanson, G.N., Shirey, S.B., 1989. Petrogenesis of mantle-derived, LILE-enriched Archean monzodiorites and trachyandesites (sanukitoids) in southwestern Superior Province. Canadian Journal of Earth Sciece 26, 1688–1712.
Sun, S.S., McDonough, W.F., 1989. Chemical and isotopic systematics of oceanic basalts: implications for mantle composition and processes. In: Saunders, A.D., Norry, M.J. (Eds.), Magmatism in the Ocean Basins: Geological Society London Special Publications, pp. 313–345.
Sun, M., Yuan, C., Xiao, W.J., Long, X.P., Xia, X.P., Zhao, G.C., Lin, S.F., Wu, F.Y., Kroner, A., 2008. Zircon U–Pb and Hf isotopic study of gneissic rocks from the Chinese Altai: progressive accretionary history in the early to middle Palaeozoic. Chemical Geology 247 (3–4), 352–383.
Tang, H.F., Zhao, Z.Q., Huang, R.S., Han, Y.J., Su, Y.P., 2008. Primary Hf isotopic study on zircons from the A-type granites in Eastern Junggar of Xinjiang, Northwest China. Acta Miner Sin 28, 335–342 (in Chinese with English abstract).
Tang, G.-J., Wang, Q., Wyman, D.A., Li, Z.-X., Zhao, Z.-H., Jia, X.-H., Jiang, Z.-Q., 2010. Ridge subduction and crustal growth in the Central Asian Orogenic Belt: evidence from Late Carboniferous adakites and high-Mg diorites in the western Junggar region, northern Xinjiang (west China). Chemical Geology 227 (3–4), 281–300.
Tang, G.J., Wang, Q., Wyman, D.A., Li, Z.X., Xu, Y.G., Zhao, Z.H., 2012. Recycling oceanic crust for continental crustal growth: Sr–Nd–Hf isotope evidence from granotoids in the western Junggar region, NW China. Lithos 128–131, 73–83.
Tang, G.-J., Wyman, D. A., Wang, Q., Li, Z.-X., Zhao, Z.-H., Sun, W.-D., Li, J., submitted for publication. Asthenosphere–lithosphere interaction triggered by a slab window during ridge subduction: trace element and Sr–Nd–Hf–Os isotopic evidence from Late Carboniferous tholeiites in the western Junggar area (NW China).
Tatsumi, Y., 2006. High-Mg andesites in the Setouchi volcanic belt, southwestern Japan: analogy to Archean magmatism and continental crust formation? Annual Review of Earth and Plantary Science 34, 467–499.
Tatsumi, Y., 2008. Making continental crust: the sanukitoid connection. Chinese Science Bulletin 53 (11), 1620–1633.
Tatsumi, Y., Ishizaka, K., 1981. Existence of andesitic primary magma: an example from southwest Japan. Earth and Planetary Science Letters 53 (1), 124–130.
Tatsumi, Y., Ishizaka, K., 1982. Origin of high-magnesian andesites in the Setouchi volcanic belt, southwest Japan, I. Petrographical and chemical characteristics. Earth and Planetary Science Letters 60 (2), 293–304.
Tatsumi, Y., Shukuno, H., Sato, K., Shibata, T., Yoshikawa, M., 2003. The petrology and geochemistry of high-magnesium andesites at the western tip of the Setouchi Volcanic Belt, SW Japan. Journal of Petrology 44 (9), 1561–1578.
Tatsumi, Y., Suzuki, T., Kawabata, H., Sato, K., Miyazaki, T., Chang, Q., Takahashi, T., Tani, K., Shibata, T., Yoshikawa, M., 2006. The petrology and geochemistry of Oto–Zan composite lava flow on Shodo-Shima Island, SW Japan: remelting of a solidified high-mg andesite magma. Journal of Petrology 47 (3), 595–629.
Taylor, S.R., McLennan, S.M., 1985. The Continental Crust: Its Composition and Evolution. Blackwell, Oxford.
Taylor, S.R., McLennan, S.M., 1995. The geochemical evolution of the continental crust. Review of Geophysics 33 (2), 241–265.
Thorkelson, D.J., 1996. Subduction of diverging plates and the principles of slab window formation. Tectonophysics 255 (1–2), 47–63.
Tiepolo, M., Tribuzio, R., 2008. Petrology and U–Pb zircon geochronology of amphibole-rich cumulates with Sanukitic affinity from Husky Ridge (Northern Victoria Land, Antarctica): insights into the role of amphibole in the petrogenesis of subduction-related magmas. Journal of Petrology 49 (5), 937–970.
Vernon, R.H., 1984. Microgranitoid enclaves in granites(mdash)globules of hybrid magma quenched in a plutonic environment. Nature 309 (5967), 438–439.
Wang, R., Zhu, Y.F., 2007. Geology of the Baobei Gold deposit in Western Juggar and zircon SHRIMP age of its wall-rocks, Western Junggar (Xinjiang, NW China). Geological Journal of China University 13 (3), 590–602.
Wang, Q., Li, Z.X., Chung, S.L., Wyman, D.A., Sun, Y.L., Zhao, Z.H., Zhu, Y.T., Qiu, H.N., 2011. Late Triassic high-Mg andesite/dacite suites from northern Hohxil, North Tibet: geochronology, geochemical characteristics, petrogenetic processes and tectonic implications. Lithos 126 (1–2), 54–67.
Watson, E.B., Harrison, T.M., 1983. Zircon saturation revisited: temperature and composition effects in a variety of crustal magma types. Earth and Planetary Science Letters 64 (2), 295–304.
Weinschenk, E., 1891. Beiträge zur Petrographie Japans. Neues Jahrbuch für Mineralogie, Geologie und Paläontologie 7, 133–151.
Whalen, J.B., Currie, K.L., Chappell, B.W., 1987. A-type granites: geochemical characteristics, discrimination and petrogenesis. Contributions to Mineralogy and Petrology 95 (4), 407–419.
Whalen, J.B., Percival, J.A., McNicoll, V.J., Longstaffe, F.J., 2004. Geochemical and isotopic (Nd–O) evidence bearing on the origin of late- to post-orogenic high-K granitoid rocks in the Western Superior Province: implications for late Archean tectonomagmatic processes. Precambrian Research 132 (3), 303–326.
Windley, B.F., Alexeiev, D., Xiao, W., Kroner, A., Badarch, G., 2007. Tectonic models for accretion of the Central Asian Orogenic Belt. The Journal of Geology Society London 164 (1), 31–47.
Wolf, M.B., Wyllie, P.J., 1994. Dehydration-melting of amphibolite at 10 kbar: the effects of temperature and time. Contributions to Mineralogy and Petrology 115 (4), 369–383.
Wu, F.Y., Jahn, B.M., Wilde, S., Sun, D.Y., 2000. Phanerozoic crustal growth: U–Pb and Sr–Nd isotopic evidence from the granites in northeastern China. Tectonophysics 328 (1–2), 89–113.
Wu, F.Y., Sun, D.Y., Li, H.M., Jahn, B.M., Wilde, S., 2002. A-type granites in northeastern China: age and geochemical constraints on their petrogenesis. Chemical Geology 187 (1–2), 143–173.
Wyman, D.A., 1999. A 2.7 Ga depleted tholeiite suite: evidence of plume–arc interaction in the Abitibi Greenstone Belt, Canada. Precambrian Research 97 (1–2), 27–42.
Wyman, D., Kerrich, R., 2009. Plume and arc magmatism in the Abitibi subprovince: implications for the origin of Archean continental lithospheric mantle. Precambrian Research 168 (1–2), 4–22.
Xiao, W.J., Windley, B.F., Hao, J., Zhai, M.G., 2003. Accretion leading to collision and the Permian Solonker suture, Inner Mongolia, China: termination of the central Asian orogenic belt. Tectonics 22 (6), 1069. doi:10.1029/2002TC001484.
Xiao, W.J., Han, C.M., Yuan, C., Sun, M., Lin, S.F., Chen, H.L., Li, Z.L., Li, J.L., Sun, S., 2008. Middle Cambrian to Permian subduction-related accretionary orogenesis of Northern Xinjiang, NW China: implications for the tectonic evolution of central Asia. Journal of Asian Earth Science 32 (2–4), 102–117.
Xu, Y.G., Lan, J.B., Yang, Q.J., Huang, X.L., Qiu, H.N., 2008. Eocene break-off of the Neo-Tethyan slab as inferred from intraplate-type mafic dykes in the Gaoligong Orogenic Belt, eastern Tibet. Chemical Geology 255 (3–4), 439–453.
Yang, J.-H., Wu, F.-Y., Chung, S.L., Wilde, S.A., Chu, M.F., 2006. A hybrid origin for the Qianshan A-type granite, northeast China: geochemical and Sr–Nd–Hf isotopic evidence. Lithos 89 (1–2), 89–106.
Yang, J.-H., Wu, F.-Y., Wilde, S.A., Liu, X.-M., 2007a. Petrogenesis of Late Triassic granitoids and their enclaves with implications for post-collisional lithospheric thinning of the Liaodong Peninsula, North China Craton. Chemical Geology 242 (1–2), 155–175.
Yang, J.-H., Wu, F.-Y., Wilde, S., Xie, L.-W., Yang, Y.-H., Liu, X.-M., 2007b. Tracing magma mixing in granite genesis: in situ U–Pb dating and Hf-isotope analysis of zircons. Contributions to Mineralogy and Petrology 153 (2), 177–190.
Yin, J., Yuan, C., Sun, M., Long, X., Zhao, G., Wong, K.P., Geng, H., Cai, K., 2010. Late Carboniferous high-Mg dioritic dikes in Western Junggar, NW China: geochemical features, petrogenesis and tectonic implications. Gondwana Research 17 (1), 145–152.
Zhang, J.E., Xiao, W.J., Han, C.M., Ao, S.J., Yuan, C., Sun, M., Geng, H.Y., Zhao, G.C., Guo, Q.Q., Ma, C., 2011a. Kinematics and age constraints of deformation in a Late Carboniferous accretionary complex in Western Junggar, NW China. Gondwana Researchearch 19 (4), 958–974.
Zhang, J.E., Xiao, W.J., Han, C.M., Mao, Q.G., Ao, S.J., Guo, Q.Q., Ma, C., 2011b. A Devonian to Carboniferous intra-oceanic subduction system in Western Junggar, NW China. Lithos 125, 592–606.